
Deep Adaptive Design: Amortizing Sequential Bayesian Experimental Design

Adam Foster^{*1} Desi R. Ivanova^{*1} Ilyas Malik² Tom Rainforth¹

Abstract

We introduce Deep Adaptive Design (DAD), a general method for amortizing the cost of performing sequential adaptive experiments using the framework of Bayesian optimal experimental design (BOED). Traditional sequential BOED approaches require substantial computational time at each stage of the experiment. This makes them unsuitable for most real-world applications, where decisions must typically be made quickly. DAD addresses this restriction by learning an amortized design network upfront and then using this to rapidly run (multiple) adaptive experiments at deployment time. This network takes as input the data from previous steps, and outputs the next design using a single forward pass; these design decisions can be made in milliseconds during the live experiment. To train the network, we introduce contrastive information bounds that are suitable objectives for the sequential setting, and propose a customized network architecture that exploits key symmetries. We demonstrate that DAD successfully amortizes the process of experimental design, outperforming alternative strategies on a number of problems.

1. Introduction

A key challenge across disciplines as diverse as psychology (Myung et al., 2013), bioinformatics (Vanlier et al., 2012), pharmacology (Lyu et al., 2019) and physics (Dushenko et al., 2020) is to design experiments so that the outcomes will be as informative as possible about the underlying process. Bayesian optimal experimental design (BOED) is a powerful mathematical framework for tackling this problem (Lindley, 1956; Chaloner & Verdinelli, 1995).

In the BOED framework, outcomes y are modeled in a Bayesian manner (Gelman et al., 2013; Kruschke, 2014) using a likelihood $p(y|\theta, \xi)$ and a prior $p(\theta)$, where ξ is

our controllable design and θ is the set of parameters we wish to learn about. We then optimize ξ to maximize the *expected information gained* about θ (equivalently the mutual information between y and θ):

$$I(\xi) := \mathbb{E}_{p(\theta)p(y|\theta, \xi)} [\log p(y|\theta, \xi) - \log p(y|\xi)]. \quad (1)$$

The true power of BOED is realized when it is used to design a sequence of experiments ξ_1, \dots, ξ_T , where it allows us to construct *adaptive* strategies which utilize information gathered from past data $\xi_1, \dots, \xi_{t-1}, y_1, \dots, y_{t-1}$ to tailor each successive design ξ_t during the progress of the experiment. The conventional approach for selecting each ξ_t is to fit the posterior $p(\theta|\xi_{1:t-1}, y_{1:t-1})$ representing the updated beliefs about θ after the first $t - 1$ iterations have been conducted, and then substitute this for the prior in (1) (Ryan et al., 2016; Rainforth, 2017; Kleinegesse et al., 2020). The design ξ_t is then chosen as the one which maximizes the resulting objective.

Unfortunately, this approach necessitates significant computational time to be expended *between each step of the experiment* in order to update the posterior and compute the next optimal design. In particular, the mutual information objective is doubly intractable (Rainforth et al., 2018; Zheng et al., 2018) and its optimization constitutes a significant computational bottleneck. This can be prohibitive to the practical application of sequential BOED; design decisions, more often than not, need to be made quickly for the approach to be useful (Evans & Mathur, 2005).

To give a concrete example, consider running an adaptive survey to understand political opinions (Pasek & Krosnick, 2010). A question ξ_t is put to a participant who gives their answer y_t and this data is used to update an underlying model with latent variables θ . Here sequential BOED is of immense value because previous answers can be used to guide future questions, ensuring that they are pertinent to the particular participant. However, it is not acceptable to have lengthy delays between questions to compute the next design, precluding existing approaches from being used.

To alleviate this problem we propose *amortizing* the cost of sequential experimental design, performing upfront training before the start of the experiment to allow very fast design decisions at deployment, when time is at a premium. This amortization is particularly useful in the typical scenario

^{*}Equal contribution ¹Department of Statistics, University of Oxford, UK ²Work undertaken whilst at the University of Oxford. Correspondence to: Adam Foster <adam.foster@stats.ox.ac.uk>.

where the same adaptive experimental framework will be deployed numerous times (e.g. having multiple participants in a survey). Adaptive experiments that are only run once are rare because they can often be dealt with manually by a human experimenter. Here amortization not only removes the computational burden from the live experiment, it also allows for sharing computation across multiple experiments, analogous to inference amortization that allows one to deal with multiple datasets (Stuhlmüller et al., 2013).

Our approach, called **Deep Adaptive Design (DAD)**, constructs a single design network which takes as input the designs and observations from previous stages, and outputs the design to use for the next experiment. The network is learned by simulating hypothetical experimental trajectories and then using these to train the network to make near-optimal design decisions automatically. That is, it learns to make design decisions as a *function* of the past data, and we optimize the parameters of this function rather than an individual design. Once learned, the network can be used repeatedly for different instantiations of the experiment (e.g. different human participants) and eliminates the computational bottleneck at each iteration for them, enabling them to be run both adaptively and quickly.

To allow for efficient, effective, and simple training, we show how DAD networks can be learned without any direct posterior or marginal likelihood estimation. This is achieved by deriving contrastive bounds that allow for end-to-end training with stochastic gradient ascent, thereby sidestepping both the need for inference and the double intractability of the mutual information objective.

We also derive a key permutation symmetry property of the optimal design function, and use this to propose a customized architecture for the experimental design network. This is critical to allowing effective amortization across time steps. The overall result of the theoretical formulation, novel contrastive bounds, and neural architecture is a training regime which enables us to bring the power of deep learning to bear on sequential experimental design.

We apply DAD to a range of problems relevant to applications such as epidemiology, physics and psychology. We find that DAD is able to accurately amortize experiments, opening the door to running adaptive BOED in real time.

2. Background

Because experimentation is a potentially costly endeavour, it is essential to design experiments so that we are likely to learn a lot from them. We adopt the BOED framework pioneered by Lindley (1956), in which the central measure of the quality of an experimental design ξ is the expected amount of *information* gained about the model latent variable θ from the observation y .

We begin with the standard Bayesian modelling set-up consisting of an explicit likelihood model $p(y|\theta, \xi)$ for the experiment, and a prior $p(\theta)$ representing our initial beliefs about the unknown latent. After running an experiment with design ξ and observing y , our updated beliefs are the posterior $p(\theta|\xi, y)$. The amount of information that has been gained about θ can be mathematically described by the reduction in entropy from the prior to the posterior

$$\text{IG}(\xi, y) = H[p(\theta)] - H[p(\theta|\xi, y)]. \quad (2)$$

The *expected information gain* (EIG) is formed by taking the expectation over the Bayesian marginal distribution for the outcome $p(y|\xi) = \mathbb{E}_{p(\theta)}[p(y|\theta, \xi)]$, yielding

$$\begin{aligned} I(\xi) &:= \mathbb{E}_{p(y|\xi)} [H[p(\theta)] - H[p(\theta|\xi, y)]] \\ &= \mathbb{E}_{p(\theta)p(y|\theta, \xi)} [\log p(\theta|\xi, y) - \log p(\theta)] \\ &= \mathbb{E}_{p(\theta)p(y|\theta, \xi)} [\log p(y|\theta, \xi) - \log p(y|\xi)] \end{aligned}$$

which is the mutual information between y and θ under design ξ . The optimal design is defined as $\xi^* = \arg \max_{\xi \in \Xi} I(\xi)$ where Ξ is the space of feasible designs.

The true power of BOED lies in its application to sequential experimentation. In this setting, we run experiments with designs ξ_1, \dots, ξ_T , observing outcomes y_1, \dots, y_T . Importantly, each ξ_t can be chosen dependent upon $\xi_{1:t-1}, y_{1:t-1}$, enabling us to use what has already been learned in previous experiments to design the next one optimally, resulting in a virtuous cycle of improving beliefs and using updated beliefs to design good experiments for future iterations.

The conventional approach to computing designs adaptively is to fit the posterior distribution $p(\theta|\xi_{1:t-1}, y_{1:t-1})$ at each step, and then optimize the mutual information objective that uses this posterior in place of the prior (Ryan et al., 2016; Rainforth, 2017; Kleingesse et al., 2020)

$$I(\xi_t) = \mathbb{E}_{p(\theta|\xi_{1:t-1}, y_{1:t-1})p(y_t|\theta, \xi_t)} \left[\log \frac{p(y_t|\theta, \xi_t)}{p(y_t|\xi_t)} \right] \quad (3)$$

where $p(y_t|\xi_t) = \mathbb{E}_{p(\theta|\xi_{1:t-1}, y_{1:t-1})}[p(y_t|\theta, \xi_t)]$.

Despite the great potential of the sequential BOED framework, this conventional approach is very computationally expensive. At each stage t of the experiment we must compute the posterior $p(\theta|\xi_{1:t-1}, y_{1:t-1})$, which is costly and cannot be done in advance as it depends on $y_{1:t-1}$. Furthermore, the posterior is then used to obtain ξ_t by maximizing the objective in (3), which is computationally even more demanding as it involves the optimization of a doubly intractable quantity (Rainforth et al., 2018; Foster et al., 2019). Both of these steps must be done during the experiment, implying that it is infeasible to run adaptive BOED in real time experiment settings unless the model is unusually simple.

2.1. Contrastive information bounds

In Foster et al. (2020), the authors noted that if $\xi \in \Xi$ is continuous, approximate optimization of the mutual information at each stage of the experiment can be achieved in a single *unified* stochastic gradient procedure that both estimates and optimizes the mutual information simultaneously. A key component of this approach is the derivation of several contrastive lower bounds on mutual information, inspired by work in representation learning (van den Oord et al., 2018; Poole et al., 2019). One such bound is the Prior Contrastive Estimation (PCE) bound, given by

$$I(\xi) \geq \mathbb{E} \left[\log \frac{p(y|\theta_0, \xi)}{\frac{1}{L+1} \sum_{\ell=0}^L p(y|\theta_\ell, \xi)} \right] \quad (4)$$

where $\theta_0 \sim p(\theta)$ is the sample used to generate $y \sim p(y|\theta, \xi)$ and $\theta_{1:L}$ are L contrastive samples drawn independently from $p(\theta)$; as $L \rightarrow \infty$ the bound becomes tight. The PCE bound can be maximized by stochastic gradient ascent (SGA) (Robbins & Monro, 1951) to approximate the optimal design ξ . As discussed previously, in a sequential setting this stochastic gradient optimization is repeated T times with $p(\theta)$ replaced by $p(\theta|\xi_{1:t-1}, y_{1:t-1})$ at step t .

3. Rethinking Sequential BOED

To enable adaptive BOED to be deployed in settings where design decisions must be taken quickly, we first need to place the standard sequential BOED approach within a formal framework for adaptive sequential design. To this end, we introduce the concept of a *design function*, or *policy*, π that maps from the set of all previous design–observation pairs to the next chosen design.

Let h_t denote the experimental *history* $(\xi_1, y_1), \dots, (\xi_t, y_t)$. We can simulate histories for a given policy π , by sampling a $\theta \sim p(\theta)$, then, for each $t = 1, \dots, T$, fixing $\xi_t = \pi(h_{t-1})$ (where $h_0 = \emptyset$) and sampling $y_t \sim p(y|\theta, \xi_t)$. The density of this generative process is given by

$$p(\theta)p(h_T|\theta, \pi) = p(\theta) \prod_{t=1}^T p(y_t|\theta, \xi_t). \quad (5)$$

The standard sequential BOED approach described in § 2 now corresponds to a costly implicit policy π_s , that performs posterior estimation followed by mutual information optimization to choose each design. By contrast, in DAD, we will learn a deterministic π that chooses designs directly.

Another way to think about π_s is that it is the policy which piecewise optimizes the following objective for $\xi_t|h_{t-1}$

$$I_{h_{t-1}}(\xi_t) := \mathbb{E}_{p(\theta|h_{t-1})p(y_t|\theta, \xi_t)} \left[\log \frac{p(y_t|\theta, \xi_t)}{p(y_t|h_{t-1}, \xi_t)} \right] \quad (6)$$

where $p(y_t|h_{t-1}, \xi_t) = \mathbb{E}_{p(\theta|h_{t-1})}[p(y_t|\theta, \xi_t)]$. It is thus the optimal *myopic* policy (that is a policy which fails to reason

about its own future actions) for an objective given by the sum of EIGs from each experiment iteration. Note that this is not the optimal *overall* policy as it fails to account for future decision making (González et al., 2016; Jiang et al., 2020).

Trying to learn an efficient policy that directly mimics π_s would be extremely computationally challenging because of the difficulties of dealing with both inference and mutual information estimation at each iteration of the training. Indeed, the natural way to do this would involve running a full, very expensive, simulated sequential BOED process to generate each training example.

We address this problem by reformulating the sequential decision problem in a way that completely eliminates the need for calculating either posterior distributions or intermediate objectives. This is done by exploiting an important property of the EIG: the total EIG of a sequential experiment is the sum of the (conditional) EIGs for each experiment iteration. This is formalized in the following result, which allows us to write down a single expression for the expected information gained from the entire sequence of T experiments.

Theorem 1. *The total expected information gain for policy π over a sequence of T experiments is*

$$\mathcal{I}_T(\pi) := \mathbb{E}_{p(\theta)p(h_T|\theta, \pi)} \left[\sum_{t=1}^T I_{h_{t-1}}(\xi_t) \right] \quad (7)$$

$$= \mathbb{E}_{p(\theta)p(h_T|\theta, \pi)} [\log p(h_T|\theta, \pi) - \log p(h_T|\pi)] \quad (8)$$

where $p(h_T|\pi) = \mathbb{E}_{p(\theta)}[p(h_T|\theta, \pi)]$.

The proof is given in Appendix A. Intuitively, the total EIG of (8) is the expected reduction in entropy from the prior $p(\theta)$ to the *final* posterior $p(\theta|h_T)$, without considering the intermediate posteriors at all. This formulation is thus key to being able to efficiently and effectively learn a policy that can, in turn, be used quickly at deployment time; our approach is to focus directly on estimating and optimizing the unified objective function $\mathcal{I}_T(\pi)$.

4. Deep Adaptive Design

Theorem 1 showed that the optimal design function $\pi^* = \arg \max_{\pi} \mathcal{I}_T(\pi)$ is the one which maximizes the mutual information between the unknown latent θ and the full rollout of histories produced using that policy, h_T . DAD looks to approximate π^* explicitly using a neural network, which we now refer to as the *design network* π_ϕ , with trainable parameters ϕ . This direct function approximation approach marks a major break from existing methods, which do not represent a policy explicitly as a function, but compute designs on the fly during the experiment.

DAD amortizes the cost of experimental design—by training the network parameters ϕ , the design network is taught to make correct design decisions across a wide range of

Algorithm 1 Deep Adaptive Design (DAD)

Input: Prior $p(\theta)$, likelihood $p(y|\theta, \xi)$, number of steps T
Output: Design network π_ϕ
while Training compute budget not exceeded **do**

 Sample $\theta_0 \sim p(\theta)$ and set $h_0 = \emptyset$

 for $t = 1, \dots, T$ **do**

 Compute $\xi_t = \pi_\phi(h_{t-1})$

 Sample $y_t \sim p(y|\theta_0, \xi_t)$

 Set $h_t = \{(\xi_1, y_1), \dots, (\xi_t, y_t)\}$

 end

 Compute estimate for $\partial \mathcal{L}_T / \partial \phi$ as per § 4.2

 Update ϕ using stochastic gradient ascent scheme

end

 At deployment time, π_ϕ is fixed and each y_t is obtained in turn by running experiment with design ξ_t .

possible experimental outcomes. This removes the cost of adaptation for the live experiment itself: during deployment the design network will select the next design nearly instantaneously with a single forward pass of the network. Further, it offers a simplification and streamlining of the sequential BOED process: it only requires the upfront end-to-end training of a single neural network and thus negates the need to set up complex *automated* inference and optimization schemes that would otherwise have to run in the background during a live experiment. A high-level summary of the DAD approach is given in Algorithm 1.

Two key technical challenges still stand in the way of realizing the potential of adaptive BOED in real time. First, whilst the unified objective $\mathcal{I}_T(\pi)$ does not require the computation of intermediate posterior distributions, it remains an intractable objective due to the presence of $p(h_T|\pi)$. To deal with this, we derive a family of lower bounds that are appropriate for the sequential experiment case and use them to construct stochastic gradient training schemes for ϕ . Second, to ensure that this network can efficiently learn a mapping from histories to designs, we require an effective architecture. As we show later, the optimal design function is invariant to the order of the history, and we use this key symmetry to maximize the effectiveness of our networks.

4.1. Contrastive bounds for sequential experiments

Our high-level aim is to train π_ϕ to maximize the mutual information $\mathcal{I}_T(\pi_\phi)$. In contrast to most machine learning tasks, this objective is *doubly* intractable and cannot be directly evaluated or even estimated with a conventional Monte Carlo estimator, except in very special cases (Rainforth et al., 2018). In fact, it is extremely challenging and costly to derive *any unbiased* estimate for it or its gradients. To train π_ϕ with stochastic gradient methods, we will therefore introduce and optimize *lower bounds* on $\mathcal{I}_T(\pi_\phi)$, building on the ideas of § 2.1.

Equation 8 shows that the objective function is the expected

logarithm of a ratio of two terms. The first is the likelihood of the history, $p(h_T|\theta, \pi)$ and can be directly evaluated using (5). The second term is an intractable marginal $p(h_T|\pi)$ that is different for each sample of the outer expectation and must thus be estimated separately each time.

Given a sample $\theta_0, h_T \sim p(\theta, h_T|\pi)$, we can perform this estimation by introducing L independent *contrastive* samples $\theta_{1:L} \sim p(\theta)$. We can then approximate the log-ratio in two different ways, depending on whether or not we include θ_0 in our estimate for $p(h_T|\pi)$:

$$g_L(\theta_{0:L}, h_T) = \log \frac{p(h_T|\theta_0, \pi)}{\frac{1}{L+1} \sum_{\ell=0}^L p(h_T|\theta_\ell, \pi)} \quad (9)$$

$$f_L(\theta_{0:L}, h_T) = \log \frac{p(h_T|\theta_0, \pi)}{\frac{1}{L} \sum_{\ell=1}^L p(h_T|\theta_\ell, \pi)}. \quad (10)$$

These forms can both be evaluated by recomputing the likelihood of the history under each of the contrastive samples $\theta_{1:L}$. We note that g cannot exceed $\log(L+1)$, whereas f is potentially unbounded.

We now show that using g to approximate the integrand leads to a *lower* bound on the overall objective $\mathcal{I}_T(\pi)$, whilst using f leads to an *upper* bound. During training, we focus on the lower bound, because it does not lead to unbounded ratio estimates and is therefore more numerically stable. We refer to this new lower bound as *sequential PCE* (sPCE).

Theorem 2 (Sequential PCE). *For a design function π and a number of contrastive samples $L \geq 0$, let*

$$\mathcal{L}_T(\pi, L) = \mathbb{E} \left[\log \frac{p(h_T|\theta_0, \pi)}{\frac{1}{L+1} \sum_{\ell=0}^L p(h_T|\theta_\ell, \pi)} \right] \quad (11)$$

where the expectation is over $\theta_0, h_T \sim p(\theta, h_T|\pi)$ and $\theta_{1:L} \sim p(\theta)$ independently. Given minor technical assumptions discussed in the proof, we have¹

$$\mathcal{L}_T(\pi, L) \uparrow \mathcal{I}_T(\pi) \text{ as } L \rightarrow \infty \quad (12)$$

at a rate $\mathcal{O}(L^{-1})$.

The proof is presented in Appendix A. For evaluation purposes, it is helpful to pair sPCE with an upper bound, which we obtain by using f as our estimate of the integrand

$$\mathcal{U}_T(\pi, L) = \mathbb{E}_{p(\theta_0, h_T|\pi)p(\theta_{1:L})} [f_L(\theta_{0:L}, h_T)]. \quad (13)$$

We refer to this bound as sequential Nested Monte Carlo (sNMC). Theorem 4 in Appendix A shows that $\mathcal{U}_T(\pi, L)$ satisfies complementary properties to $\mathcal{L}_T(\pi, L)$. In particular, $\mathcal{L}_T(\pi, L) \leq \mathcal{I}_T(\pi) \leq \mathcal{U}_T(\pi, L)$ and both bounds become monotonically tighter as L increases, becoming exact as

¹ $x_L \uparrow x$ means that x_L is a monotonically increasing sequence in L with limit x .

$L \rightarrow \infty$ at a rate $\mathcal{O}(1/L)$. We can thus directly control the trade-off between bias in our objective and the computational cost of training. Note that increasing L has no impact on the cost at deployment time. Critically, as we will see in our experiments, we tend to only need relatively modest values of L for $\mathcal{L}_T(\pi, L)$ to be an effective objective.

If using a sufficiently large L during training proves problematic (e.g. our available training time is strictly limited), one can further tighten these bounds for a fixed L by introducing an amortized proposal, $q(\theta; h_T)$, for the contrastive samples $\theta_{1:L}$, rather than drawing them from the prior. By appropriately adapting $\mathcal{L}_T(\pi, L)$, this can then be trained simultaneously to the design network itself with a single unified objective, in a manner similar to a variational autoencoder (Kingma & Welling, 2014), allowing the bound itself to get tighter during training. The resulting more general class of bounds are described in detail in Appendix B and may offer further improvements for the DAD approach. We focus on training with sPCE here in the interest of simplicity of both exposition and implementation.

4.2. Gradient estimation

We optimize the design network parameters ϕ using a stochastic optimization scheme such as Adam (Kingma & Ba, 2014). For this, we need to take gradients of the sPCE objective (11). Throughout, we assume that design space Ξ is continuous. Initially, we also assume that the observation space \mathcal{Y} is continuous and that $p(y|\theta, \xi)$ is reparametrizable. This means that we can introduce random variables $\epsilon_{1:T} \sim p(\epsilon)$, which are independent of $\xi_{1:T}$ and $\theta_{0:L}$ such that we can write $y_t = y(\theta_0, \xi_t, \epsilon_t)$. As we already have that $\xi_t = \pi_\phi(h_{t-1})$, we see that h_t becomes a deterministic function of h_{t-1} given ϵ_t and θ_0 . Under these assumptions, we can thus write²

$$\frac{d\mathcal{L}_T(\pi_\phi, L)}{d\phi} = \mathbb{E}_{p(\theta_{0:L})p(\epsilon_{1:T})} \left[\frac{dg_L(\theta_{0:L}, h_T)}{d\phi} \right]. \quad (14)$$

We can now straightforwardly construct SGA updates by sampling from $p(\theta_{0:L})p(\epsilon_{1:T})$ and evaluating $dg_L(\theta_{0:L}, h_T)/d\phi$. This can be computed via an automatic differentiation framework (Baydin et al., 2018; Paszke et al., 2019) and, using the chain rule for total derivatives and the shorthands $g = g_L(\theta_{0:L}, h_T)$ and $u_t = (\xi_t, y_t)$, is given by

$$\frac{dg}{d\phi} = \sum_{t=1}^T \frac{\partial g}{\partial u_t} \frac{du_t}{d\phi} \quad (15)$$

$$= \sum_{\substack{k \in \{1, \dots, T\} \\ 1 \leq t_1 < \dots < t_k \leq T}} \frac{\partial g}{\partial u_{t_k}} \left(\prod_{j=1}^{k-1} \frac{\partial u_{t_{j+1}}}{\partial u_{t_j}} \right) \frac{\partial u_{t_1}}{\partial \phi} \quad (16)$$

²We use $\partial a/\partial b$ and da/db to represent the Jacobian matrices of partial and total derivatives respectively for vectors a and b .

where the sum is over all $k \in \{1, \dots, T\}$ and all increasing sequences of length k in the range $1, \dots, T$, and an empty product is, by convention, equal to 1. See Appendix C for a derivation and complete description of this gradient.

Whilst this total gradient is suitable for small to moderate values of T , we found that the product term in (16) may sometimes lead to a training instability akin to the problem of exploding gradients (Hochreiter, 1991; Hochreiter & Schmidhuber, 1997). To mitigate these effects, we also propose an alternative gradient scheme that uses the partial derivative instead of the total derivative for u_t w.r.t. ϕ , thus taking into account only the direct dependence of each u_t on ϕ , yielding

$$\frac{\partial g}{\partial \phi} = \sum_{t=1}^T \frac{\partial g}{\partial u_t} \frac{\partial u_t}{\partial \phi}. \quad (17)$$

Intuitively, what this means is that we follow the gradient that individually improves the design–observation pairs u_t whilst treating other data pairs as fixed. Thus u_t will be updated to improve the history h_T in way that accounts for other $u_{s \neq t}$ in terms of their combined effect on $\mathcal{L}_T(\pi_\phi, L)$, but not in terms of the knock-on effects that changing an earlier design would have on changing the later designs π would select. This is conceptually similar to Jiang et al. (2020), in which the existence of future steps is accounted for, but not their functional dependence.

Using an analogous estimator to (17) we extend the gradient estimation to the case where y_t are discrete/categorical variables (see Appendix C). Crucially, this estimator does not induce high variance estimates that typically plague such settings (Schulman et al., 2015). We found that this training scheme was highly stable across a range of values for T .

4.3. Architecture

Finally, we discuss the deep learning architecture used for π_ϕ . To allow efficient and effective training, we take into account a key permutation invariance of the BOED problem as highlighted by the following result (proved in Appendix A).

Theorem 3 (Permutation invariance). *Consider a permutation $\sigma \in S_k$ acting on a history h_k^1 , yielding $h_k^2 = (\xi_{\sigma(1)}, y_{\sigma(1)}), \dots, (\xi_{\sigma(k)}, y_{\sigma(k)})$. For all such σ , we have*

$$\mathbb{E} \left[\sum_{t=1}^T I_{h_{t-1}}(\xi_t) \middle| h_k = h_k^1 \right] = \mathbb{E} \left[\sum_{t=1}^T I_{h_{t-1}}(\xi_t) \middle| h_k = h_k^2 \right]$$

showing that the EIG is unchanged under permutation. Further, the optimal policies starting in h_k^1 and h_k^2 are the same.

This permutation invariance is an important and well-studied property of many machine learning problems (Bloem-Reddy & Teh, 2019). The knowledge that a system exhibits permutation invariance can be exploited in neural architecture

design to enable significant *weight sharing*. One common approach is pooling (Edwards & Storkey, 2016; Zaheer et al., 2017; Garnelo et al., 2018a;b). This involves summing or otherwise combining representations of multiple inputs into a single representation that is invariant to their order.

Using this idea, we represent the history h_t with a fixed dimensional representation that is formed by pooling representations of the distinct design–outcome pairs of the history

$$R(h_t) := \sum_{k=1}^t E_{\phi_1}(\xi_k, y_k), \quad (18)$$

where E_{ϕ_1} is a neural network *encoder* with parameters ϕ_1 to be learned. Note that this pooled representation is the same if we reorder the labels $1, \dots, t$. By convention, the sum of an empty sequence is 0.

We then construct our design network to make decisions based on the pooled representation $R(h_t)$ by setting $\pi_{\phi}(h_t) = F_{\phi_2}(R(h_t))$, where F_{ϕ_2} is a learned *emitter* network. The trainable parameters are $\phi = \{\phi_1, \phi_2\}$. By combining simple networks in a way that is sensitive to the permutation invariance of the problem, we facilitate parameter sharing in which the network E_{ϕ_1} is re-used for each input pair and for each time step t . This results in significantly improved performance compared to networks that are forced to *learn* the relevant symmetries of the problem.

5. Related Work

Existing approaches to sequential BOED typically follow the path outlined in § 2. The posterior inference that is performed at each stage of the conventional approach has been done using sequential Monte Carlo (SMC) (Del Moral et al., 2006; Drovandi et al., 2014), population Monte Carlo (PMC) (Rainforth, 2017), variational inference (Foster et al., 2019), and Laplace approximations (Lewi et al., 2009; Long et al., 2013). The estimation of the mutual information objective at each step has been performed by nested Monte Carlo (Myung et al., 2013; Vincent & Rainforth, 2017), variational bounds (Foster et al., 2019), Laplace approximation (Lewi et al., 2009), ratio estimation (Kleingesse et al., 2020), and hybrid methods (Senarathne et al., 2020). The optimization over designs has been performed by Bayesian optimization (Kleingesse et al., 2020), interacting particle systems (Amzal et al., 2006), simulated annealing (Müller, 2005), utilizing regret bounds (Zheng et al., 2020), or bandit methods (Rainforth, 2017). The mutual information estimation and optimization can be combined into a single stochastic gradient procedure, with gradients estimated by perturbation analysis (Huan & Marzouk, 2014), variational lower bounds (Foster et al., 2020), or multi-level Monte Carlo (Goda et al., 2020). Other work has sought to learn a non-myopic strategy focusing on specific tractable cases (Huan & Marzouk, 2016; Jiang et al., 2020).

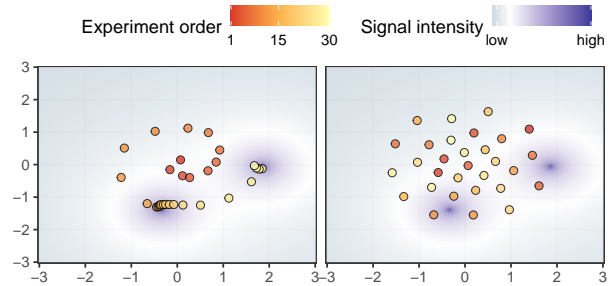


Figure 1. An example of the designs learnt by DAD [Left] and the fixed baseline [Right] for a given θ sampled from the prior.

6. Experiments

We now compare **DAD** to a number of baselines across a range of real-world experimental design problems. As our aim is to adapt designs in *real-time*, we primarily compare to strategies that are fast at deployment time. This includes **random** design and a **fixed** design strategy in which we learn T constants, ξ_1, \dots, ξ_T , before beginning the experiment, giving a non-adaptive strategy. We also compare to tailor-made heuristics for particular models as appropriate. We implement DAD by extending PyTorch (Paszke et al., 2019) and Pyro (Bingham et al., 2018) to provide an implementation that is abstracted from the specific probabilistic model. Code is provided in the Supplement.

Similarly to the notion of amortization gap in amortized inference (Cremer et al., 2018), one would expect to see a gap between the performance of DAD and that of conventional (non-amortized) BOED methods that use the approach of § 2. To assess this we also compare DAD to the **variational** method of Foster et al. (2020) that optimizes over one-step designs using SGA. We also look at several baselines that are specifically tailored to the examples that we choose (Vincent & Rainforth, 2017; Kleingesse et al., 2020). Rather surprisingly, we find that DAD is not only competitive compared to these non-amortized methods, but on occasions outperforms them. We discuss why in § 7.

The first performance metric that we focus on is total EIG, $\mathcal{I}_T(\pi)$. When no direct estimate of $\mathcal{I}_T(\pi)$ is available, we estimate both the sPCE lower bound and sNMC upper bound. We also present the standard error to indicate how the performance varies between different experiment realizations. We further consider the deployment time (i.e. the time to run the experiment itself); a critical metric for our aims. Full experiment details are given in Appendix D.

6.1. Location finding in 2D

Inspired by the acoustic energy attenuation model of Sheng & Hu (2005), we consider the problem of finding the locations of multiple hidden sources which each emits a signal whose intensity attenuates according to the inverse-square law. The *total intensity* is a superposition of these signals.

Method	Lower bound, \mathcal{L}_{30}	Upper bound, \mathcal{U}_{30}
Random	8.30 ± 0.04	8.32 ± 0.04
Fixed	8.84 ± 0.04	8.91 ± 0.04
DAD	9.94 ± 0.05	10.40 ± 0.07
Variational	8.78 ± 0.14	9.06 ± 0.19

Table 1. Upper and lower bounds on the total information, $\mathcal{I}_{30}(\pi)$, for the location finding experiment. Errors indicate ± 1 s.e. estimated over 256 (variational) or 2048 (others) rollouts.

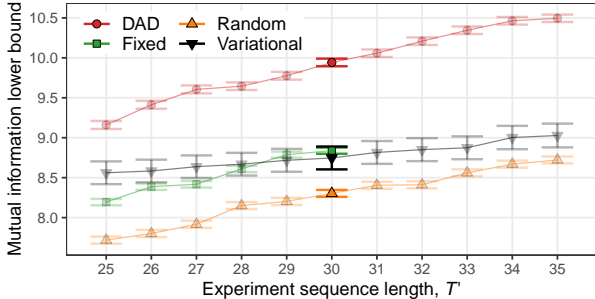


Figure 2. Generalizing sequence length for the location finding experiment. The DAD network and the fixed strategy were trained to perform $T = 30$ experiments, whilst other strategies do not require pre-training. The fixed strategy cannot be generalized to sequences longer than its training regime. We present sPCE estimates with error bars computed as in Table 1.

The design problem is to choose where to make observations of the total signal to learn the locations of the sources.

We train a DAD network to perform $T = 30$ experiments with $K = 2$ sources. The designs learned by DAD are visualized in Figure 1 [Left]. Here our network learns a complex strategy that initially explores in a spiral pattern. Once it detects a strong signal, multiple experiments are performed close together to refine knowledge of that location. This process is repeated to learn about the second source. The fixed design strategy, displayed in Figure 1 [Right] must choose all design locations up front, leading to an evenly dispersed strategy that cannot “hone in” on the critical areas, thus gathering less information.

Table 1 reports upper and lower bounds on $\mathcal{I}_T(\pi)$ for each strategy and confirms that DAD significantly outperforms the fixed and random strategies. Surprisingly, the variational posterior baseline, which requires substantial computational resources at each step of the experiment, performs notably worse than DAD; we discuss this in Section 7.

In practical situations the exact number of experiments to perform may be unknown. Figure 2 indicates that our DAD network that is pretrained to perform $T = 30$ experiments can generalize well to perform $T' \neq 30$ experiments at deployment time, still outperforming the baselines, indicating that DAD is robust to the length of training sequences. In Appendix D.1 we also show that the performance of DAD is stable across different training runs.

Method	Deployment time (s)
Frye et al. (2016)	0.0902 ± 0.0003
Kirby (2009)	0.0059 ± 0.0003
Fixed	0.0048 ± 0.0002
DAD	0.0844 ± 0.0005
Badapted (fast)	4.3055 ± 0.0339
Badapted (slow)	25.2679 ± 0.1854

Table 2. Deployment times for Hyperbolic Temporal Discounting methods. We present the total design time for $T = 20$ questions, taking the mean and ± 1 s.e. over 10 realizations. Tests were conducted on a lightweight CPU (see Appendix D).

Method	Lower bound	Upper bound
Frye et al. (2016)	3.308 ± 0.015	3.322 ± 0.015
Kirby (2009)	1.861 ± 0.008	1.864 ± 0.009
Fixed	2.518 ± 0.007	2.524 ± 0.007
DAD	4.241 ± 0.011	4.263 ± 0.012
Badapted (fast)	3.985 ± 0.014	4.019 ± 0.015
Badapted (slow)	4.454 ± 0.016	4.536 ± 0.018

Table 3. Final lower and upper bounds on the total information $\mathcal{I}_T(\pi)$ for the Hyperbolic Temporal Discounting experiment. The bounds are finite sample estimates of $\mathcal{L}_T(\pi, L)$ and $\mathcal{U}_T(\pi, L)$ with $L = 5000$. The errors indicate ± 1 s.e. over the sampled histories.

6.2. Hyperbolic temporal discounting

In psychology, temporal discounting is the phenomenon that the perceived value of an item decreases the longer we have to wait to receive it (Critchfield & Kollins, 2001; Green & Myerson, 2004). For example, a participant might be willing to trade £90 today for £100 in a month’s time, but not for £100 in a year. A common parametric model for temporal discounting in humans is the hyperbolic model (Mazur, 1987), we study a specific form of this model proposed by Vincent (2016); Vincent & Rainforth (2017). The model is described in detail in Appendix D.

We design a sequence of $T = 20$ experiments, each taking the form of a binary question “Would you prefer £ R today, or £100 in D days?” with design $\xi = (R, D)$ that must be chosen at each stage. As real applications of this model would involve human participants, the available time to choose designs is strictly limited. We consider DAD, the aforementioned fixed design policy, and strategies that have been used specifically for experiments of this kind. Kirby (2009) proposed a hand-picked fixed design; Frye et al. (2016) proposed a problem-specific adaptive strategy; Vincent & Rainforth (2017) developed a partially customized sequential BOED method, called Badapted, that uses PMC (Cappé et al., 2004) to approximate the posterior distribution at each step and a bandit approach to optimize the EIG.

We begin by investigating the time required to deploy each of these methods. As shown in Table 2, the non-amortized Badapted method takes the longest time, and we consider

Method	Deployment time (s)	$\mathcal{I}_T(\pi)$
Fixed	$0.0009 \pm 11\%$	2.023 ± 0.007
DAD	$0.0051 \pm 12\%$	2.119 ± 0.008
Variational	$1935.0 \pm 2\%$	2.076 ± 0.034
SeqBED*	25911.0	1.590

Table 4. Total EIG $\mathcal{I}_T(\pi)$ and deployment times for the Death Process. We present the EIG ± 1 s.e. over 10,000 rollouts (fixed and DAD), 500 rollouts (variational) or *1 rollout (SeqBED). The IG can be efficiently evaluated in this case (see Appendix D). Runtimes computed as per Table 2.

two different computational budgets for it based on different numbers of PMC steps. For DAD, the total design time is less than 0.1 seconds—almost imperceptible to a participant.

Table 3 shows the performance of each method. Excluding the slow Badapted method, we see that DAD performs best, outperforming bespoke design methods that have been proposed for this problem. The slower Badapted method outperforms DAD by a small margin due to its larger computation budget. This experiment demonstrates that DAD can successfully amortize the process of experimental design. It reaches a performance approaching that of the most successful non-amortized and highly problem-specific approach with a fraction of the cost during the real experiment.

6.3. Death process

We conclude with an example from epidemiology (Cook et al., 2008) in which healthy individuals become infected at rate θ . The design problem is to choose observations times $\xi > 0$ at which to observe the number of infected individuals, selecting $T = 4$ designs sequentially with an independent stochastic process observed at each iteration. We compare to SeqBED (Kleinegesse et al., 2020), a fixed design, and a variational BOED baseline.

First, we examine the compute time required to deploy each method for a single run of the sequential experiment. The times illustrated in Table 4 show that the adaptive strategy learned by DAD can be deployed in under 0.01 seconds, many orders of magnitude faster than the non-amortized methods, with SeqBED taking hours for *one* rollout.

Next, we estimate the objective $\mathcal{I}_T(\pi)$ by averaging the information gain over simulated rollouts. The results in Table 4 reveal that DAD designs are superior to both fixed design and variational adaptive design, tending to uncover more information about the latent θ across many possible experimental trajectories. For comparison with SeqBED, we were unable to perform sufficient rollouts to obtain a high quality estimate of $\mathcal{I}_T(\pi)$. Instead, we conducted a single rollout of each method with $\theta = 1.5$ fixed. The resulting information gains for this one rollout were: 1.590 (SeqBED), 1.719 (Variational), 1.6780 (Fixed), **1.772 (DAD)**.

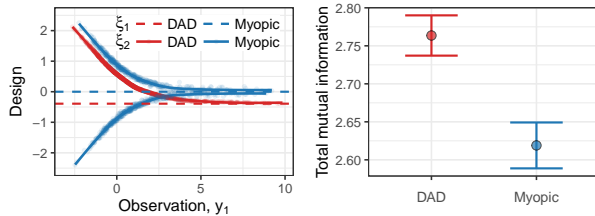


Figure 3. 1D location finding with 1 source, $T = 2$. [Left] the design function, dashed lines correspond to the first design ξ_1 , which is independent of y_1 . [Right] $\mathcal{I}_2(\pi)$, the total EIG ± 1 s.e.

7. Discussion

In this paper we introduced DAD—a new method utilizing the power of deep learning to amortize the cost of sequential BOED and allow adaptive experiments to be run in real time. In all experiments DAD performed significantly better than baselines with a comparable deployment time. Further, DAD showed competitive performance against conventional BOED approaches that do not use amortization, but make costly computations at each stage of the experiment.

Surprisingly, we found DAD was often able to outperform these non-amortized approaches despite using a tiny fraction of the resources at deployment time. We suggest two reasons for this. Firstly, conventional methods must approximate the posterior $p(\theta|h_t)$ at each stage. If this approximation is poor, the resulting design optimization will yield poor results regardless of the EIG optimization approach chosen. Careful tuning of the posterior approximation could alleviate this, but would increase computational time further and it is difficult to do this in the required automated manner. DAD sidesteps this problem altogether by eliminating the need for directly approximating a posterior distribution.

Secondly, the policy learnt by DAD has the potential to be *non-myopic*: it does not choose a design that is optimal for the current experiment in isolation, but takes into account the fact that there are more experiments to be performed in the future. We can see this in practice in a simple experiment using the location finding example with one source in 1D with prior $\theta \sim N(0, 1)$ and with $T = 2$ steps. This setting is simple enough to compute the *exact* one-step optimal design via numerical integration. Figure 3 [Left] shows the design function learnt by DAD alongside the exact optimal myopic design. The optimal myopic strategy for $t = 1$ is to sample at the prior mean $\xi_1 = 0$. At time $t = 2$ the myopic strategy selects a positive or negative design with equal probability. In contrast, the policy learnt by DAD is to sample at $\xi_1 \approx -0.4$, which does not optimize the EIG for $T = 1$ in isolation, but leads to a better *overall* design strategy that focuses on searching the positive regime $\xi_2 > \xi_1$ in the second experiment. Figure 3 [Right] confirms that the policy learned by DAD achieves higher total EIG from the two step experiment than the *exact* myopic approach.

Acknowledgements

AF gratefully acknowledges funding from EPSRC grant no. EP/N509711/1. DRI is supported by EPSRC through the Modern Statistics and Statistical Machine Learning (StatML) CDT programme, grant no. EP/S023151/1.

References

- Amzal, B., Bois, F. Y., Parent, E., and Robert, C. P. Bayesian-optimal design via interacting particle systems. *Journal of the American Statistical Association*, 101(474): 773–785, 2006.
- Angelova, J. A. On moments of sample mean and variance. *Int. J. Pure Appl. Math*, 79(1):67–85, 2012.
- Baydin, A. G., Pearlmutter, B. A., Radul, A. A., and Siskind, J. M. Automatic differentiation in machine learning: a survey. *Journal of machine learning research*, 18, 2018.
- Bingham, E., Chen, J. P., Jankowiak, M., Obermeyer, F., Pradhan, N., Karaletsos, T., Singh, R., Szerlip, P., Horsfall, P., and Goodman, N. D. Pyro: Deep universal probabilistic programming. *Journal of Machine Learning Research*, 2018.
- Bloem-Reddy, B. and Teh, Y. W. Probabilistic symmetry and invariant neural networks. *arXiv preprint arXiv:1901.06082*, 2019.
- Cappé, O., Guillin, A., Marin, J.-M., and Robert, C. P. Population monte carlo. *Journal of Computational and Graphical Statistics*, 13(4):907–929, 2004.
- Chaloner, K. and Verdinelli, I. Bayesian experimental design: A review. *Statistical Science*, pp. 273–304, 1995.
- Cook, A. R., Gibson, G. J., and Gilligan, C. A. Optimal observation times in experimental epidemic processes. *Biometrics*, 64(3):860–868, 2008.
- Cremer, C., Li, X., and Duvenaud, D. Inference suboptimality in variational autoencoders. In *Proceedings of the 35th International Conference on Machine Learning*, volume 80 of *Proceedings of Machine Learning Research*, pp. 1078–1086. PMLR, 2018.
- Critchfield, T. S. and Kollins, S. H. Temporal discounting: Basic research and the analysis of socially important behavior. *Journal of applied behavior analysis*, 34(1): 101–122, 2001.
- Del Moral, P., Doucet, A., and Jasra, A. Sequential monte carlo samplers. *Journal of the Royal Statistical Society: Series B (Statistical Methodology)*, 68(3):411–436, 2006.
- Drovandi, C. C., McGree, J. M., and Pettitt, A. N. A sequential monte carlo algorithm to incorporate model uncertainty in bayesian sequential design. *Journal of Computational and Graphical Statistics*, 23(1):3–24, 2014.
- Dushenko, S., Ambal, K., and McMichael, R. D. Sequential bayesian experiment design for optically detected magnetic resonance of nitrogen-vacancy centers. *Physical Review Applied*, 14(5):054036, 2020.
- Edwards, H. and Storkey, A. Towards a neural statistician. *arXiv preprint arXiv:1606.02185*, 2016.
- Evans, J. R. and Mathur, A. The value of online surveys. *Internet research*, 2005.
- Foster, A., Jankowiak, M., Bingham, E., Horsfall, P., Teh, Y. W., Rainforth, T., and Goodman, N. Variational Bayesian Optimal Experimental Design. In *Advances in Neural Information Processing Systems 32*, pp. 14036–14047. Curran Associates, Inc., 2019.
- Foster, A., Jankowiak, M., O’Meara, M., Teh, Y. W., and Rainforth, T. A unified stochastic gradient approach to designing bayesian-optimal experiments. volume 108 of *Proceedings of Machine Learning Research*, pp. 2959–2969, Online, 26–28 Aug 2020. PMLR.
- Frye, C. C., Galizio, A., Friedel, J. E., DeHart, W. B., and Odum, A. L. Measuring delay discounting in humans using an adjusting amount task. *JoVE (Journal of Visualized Experiments)*, (107):e53584, 2016.
- Garnelo, M., Rosenbaum, D., Maddison, C. J., Ramalho, T., Saxton, D., Shanahan, M., Teh, Y. W., Rezende, D. J., and Eslami, S. Conditional neural processes. *arXiv preprint arXiv:1807.01613*, 2018a.
- Garnelo, M., Schwarz, J., Rosenbaum, D., Viola, F., Rezende, D. J., Eslami, S., and Teh, Y. W. Neural processes. *arXiv preprint arXiv:1807.01622*, 2018b.
- Gelman, A., Carlin, J. B., Stern, H. S., Dunson, D. B., Vehtari, A., and Rubin, D. B. *Bayesian data analysis*. Chapman and Hall/CRC, 2013.
- Goda, T., Hironaka, T., and Kitade, W. Unbiased mlmc stochastic gradient-based optimization of bayesian experimental designs. *arXiv preprint arXiv:2005.08414*, 2020.
- González, J., Osborne, M., and Lawrence, N. Glasses: Relieving the myopia of bayesian optimisation. In *Artificial Intelligence and Statistics*, pp. 790–799. PMLR, 2016.
- Green, L. and Myerson, J. A discounting framework for choice with delayed and probabilistic rewards. *Psychological bulletin*, 130(5):769, 2004.

- Hochreiter, S. Untersuchungen zu dynamischen neuronalen netzen. *Diploma, Technische Universität München*, 91 (1), 1991.
- Hochreiter, S. and Schmidhuber, J. Long short-term memory. *Neural computation*, 9(8):1735–1780, 1997.
- Huan, X. and Marzouk, Y. Gradient-based stochastic optimization methods in bayesian experimental design. *International Journal for Uncertainty Quantification*, 4(6), 2014.
- Huan, X. and Marzouk, Y. M. Sequential bayesian optimal experimental design via approximate dynamic programming. *arXiv preprint arXiv:1604.08320*, 2016.
- Jiang, S., Chai, H., Gonzalez, J., and Garnett, R. Binoculars for efficient, nonmyopic sequential experimental design. In *International Conference on Machine Learning*, pp. 4794–4803. PMLR, 2020.
- Kingma, D. P. and Ba, J. Adam: A method for stochastic optimization. *arXiv preprint arXiv:1412.6980*, 2014.
- Kingma, D. P. and Welling, M. Auto-encoding variational Bayes. In *ICLR*, 2014.
- Kirby, K. N. One-year temporal stability of delay-discount rates. *Psychonomic bulletin & review*, 16(3):457–462, 2009.
- Kleinegesse, S., Drovandi, C., and Gutmann, M. U. Sequential bayesian experimental design for implicit models via mutual information. *arXiv preprint arXiv:2003.09379*, 2020.
- Kruschke, J. Doing bayesian data analysis: A tutorial with r, jags, and stan. 2014.
- Lewi, J., Butera, R., and Paninski, L. Sequential optimal design of neurophysiology experiments. *Neural Computation*, 21(3):619–687, 2009.
- Lindley, D. V. On a measure of the information provided by an experiment. *The Annals of Mathematical Statistics*, pp. 986–1005, 1956.
- Long, Q., Scavino, M., Tempone, R., and Wang, S. Fast estimation of expected information gains for Bayesian experimental designs based on Laplace approximations. *Computer Methods in Applied Mechanics and Engineering*, 259:24–39, 2013.
- Lyu, J., Wang, S., Balius, T. E., Singh, I., Levit, A., Moroz, Y. S., O’Meara, M. J., Che, T., Algaa, E., Tolmachova, K., et al. Ultra-large library docking for discovering new chemotypes. *Nature*, 566(7743):224, 2019.
- Mazur, J. E. An adjusting procedure for studying delayed reinforcement. *Commons, ML.; Mazur, JE.; Nevin, JA*, pp. 55–73, 1987.
- Müller, P. Simulation based optimal design. *Handbook of Statistics*, 25:509–518, 2005.
- Myung, J. I., Cavagnaro, D. R., and Pitt, M. A. A tutorial on adaptive design optimization. *Journal of mathematical psychology*, 57(3-4):53–67, 2013.
- Nowozin, S. Debiasing evidence approximations: On importance-weighted autoencoders and jackknife variational inference. In *International Conference on Learning Representations*, 2018.
- Pasek, J. and Krosnick, J. A. Optimizing survey questionnaire design in political science. In *The Oxford handbook of American elections and political behavior*. 2010.
- Paszke, A., Gross, S., Massa, F., Lerer, A., Bradbury, J., Chanan, G., Killeen, T., Lin, Z., Gimelshein, N., Antiga, L., Desmaison, A., Kopf, A., Yang, E., DeVito, Z., Raison, M., Tejani, A., Chilamkurthy, S., Steiner, B., Fang, L., Bai, J., and Chintala, S. Pytorch: An imperative style, high-performance deep learning library. In *Advances in Neural Information Processing Systems 32*, pp. 8024–8035. Curran Associates, Inc., 2019.
- Poole, B., Ozair, S., van den Oord, A., Alemi, A., and Tucker, G. On variational bounds of mutual information. In *International Conference on Machine Learning*, pp. 5171–5180, 2019.
- Rainforth, T. *Automating Inference, Learning, and Design using Probabilistic Programming*. PhD thesis, University of Oxford, 2017.
- Rainforth, T., Cornish, R., Yang, H., Warrington, A., and Wood, F. On nesting monte carlo estimators. In *International Conference on Machine Learning*, pp. 4267–4276. PMLR, 2018.
- Robbins, H. and Monro, S. A stochastic approximation method. *The annals of mathematical statistics*, pp. 400–407, 1951.
- Ryan, E. G., Drovandi, C. C., McGree, J. M., and Pettitt, A. N. A review of modern computational algorithms for bayesian optimal design. *International Statistical Review*, 84(1):128–154, 2016.
- Schulman, J., Heess, N., Weber, T., and Abbeel, P. Gradient estimation using stochastic computation graphs. In *Advances in Neural Information Processing Systems*, 2015.
- Senarathne, S., Drovandi, C., and McGree, J. A laplace-based algorithm for bayesian adaptive design. *Statistics and Computing*, 30(5):1183–1208, 2020.

- Sheng, X. and Hu, Y. H. Maximum likelihood multiple-source localization using acoustic energy measurements with wireless sensor networks. *IEEE Transactions on Signal Processing*, 2005. ISSN 1053587X. doi: 10.1109/TSP.2004.838930.
- Stuhlmüller, A., Taylor, J., and Goodman, N. Learning stochastic inverses. In *Advances in neural information processing systems*, pp. 3048–3056, 2013.
- van den Oord, A., Li, Y., and Vinyals, O. Representation learning with contrastive predictive coding. *arXiv preprint arXiv:1807.03748*, 2018.
- Vanlier, J., Tiemann, C. A., Hilbers, P. A., and van Riel, N. A. A Bayesian approach to targeted experiment design. *Bioinformatics*, 28(8):1136–1142, 2012.
- Vincent, B. T. Hierarchical bayesian estimation and hypothesis testing for delay discounting tasks. *Behavior research methods*, 48(4):1608–1620, 2016.
- Vincent, B. T. and Rainforth, T. The DARC toolbox: automated, flexible, and efficient delayed and risky choice experiments using bayesian adaptive design. 2017.
- Zaheer, M., Kottur, S., Ravanbakhsh, S., Poczos, B., Salakhutdinov, R., and Smola, A. Deep sets. *arXiv preprint arXiv:1703.06114*, 2017.
- Zheng, S., Pacheco, J., and Fisher, J. A robust approach to sequential information theoretic planning. In *International Conference on Machine Learning*, pp. 5941–5949, 2018.
- Zheng, S., Hayden, D., Pacheco, J., and Fisher III, J. W. Sequential bayesian experimental design with variable cost structure. *Advances in Neural Information Processing Systems*, 33, 2020.

A. Proofs

Here we present proofs for all Theorems in the main paper, with each restated for convenience.

Theorem 1. *The total expected information gain for policy π over a sequence of T experiments is*

$$\mathcal{I}_T(\pi) := \mathbb{E}_{p(\theta)p(h_T|\theta,\pi)} \left[\sum_{t=1}^T I_{h_{t-1}}(\xi_t) \right] \quad (7)$$

$$= \mathbb{E}_{p(\theta)p(h_T|\theta,\pi)} [\log p(h_T|\theta, \pi) - \log p(h_T|\pi)] \quad (8)$$

where $p(h_T|\pi) = \mathbb{E}_{p(\theta)}[p(h_T|\theta, \pi)]$.

Proof. We begin by rewriting $I_{h_{t-1}}$ in terms of the information gain. This closely mimics the development that we presented in Section 2. By repeated application of Bayes Theorem we have

$$I_{h_{t-1}}(\xi_t) = \mathbb{E}_{p(\theta|h_{t-1})p(y_t|\theta,\xi_t)} \left[\log \frac{p(y_t|\theta, \xi_t)}{p(y_t|h_{t-1}, \xi_t)} \right] \quad (19)$$

$$= \mathbb{E}_{p(\theta|h_{t-1})p(y_t|\theta,\xi_t)} \left[\log \frac{p(\theta|h_{t-1})p(y_t|\theta, \xi_t)}{p(\theta|h_{t-1})p(y_t|h_{t-1}, \xi_t)} \right] \quad (20)$$

$$= \mathbb{E}_{p(\theta|h_{t-1})p(y_t|\theta,\xi_t)} \left[\log \frac{p(\theta|h_{t-1}, \xi_t, y_t)}{p(\theta|h_{t-1})} \right] \quad (21)$$

$$= \mathbb{E}_{p(\theta|h_{t-1})} [-\log p(\theta|h_{t-1})] + \mathbb{E}_{p(y_t,\theta|\xi_t,h_{t-1})} [\log p(\theta|h_{t-1}, \xi_t, y_t)] \quad (22)$$

$$= \mathbb{E}_{p(\theta|h_{t-1})} [-\log p(\theta|h_{t-1})] + \mathbb{E}_{p(y_t|\xi_t,h_{t-1})p(\theta|h_{t-1},\xi_t,y_t)} [\log p(\theta|h_{t-1}, \xi_t, y_t)] \quad (23)$$

$$= \mathbb{E}_{p(y_t|\xi_t,h_{t-1})} [H[p(\theta|h_{t-1})] - H[p(\theta|h_{t-1}, \xi_t, y_t)]] \quad (24)$$

Now noting that each $I_{h_{t-1}}(\xi_t)$ is completely determined by h_{t-1} and π (in particular noting that ξ_t is deterministic given these, while θ is already marginalized out in each $I_{h_{t-1}}(\xi_t)$), we can write

$$\mathcal{I}_T(\pi) = \mathbb{E}_{p(h_T|\pi)} \left[\sum_{t=1}^T I_{h_{t-1}}(\xi_t) \right] \quad (25)$$

$$= \sum_{t=1}^T \mathbb{E}_{p(h_{t-1}|\pi)} [I_{h_{t-1}}(\xi_t)] \quad (26)$$

and substituting in our earlier formulation for $I_{h_{t-1}}(\xi_t)$

$$= \sum_{t=1}^T \mathbb{E}_{p(h_{t-1}|\pi)} [\mathbb{E}_{p(y_t|\xi_t,h_{t-1})} [H[p(\theta|h_{t-1})] - H[p(\theta|h_{t-1}, \xi_t, y_t)]]] \quad (27)$$

We now observe that we can write $h_t = h_{t-1} \cup \{(\xi_t, y_t)\}$, which allows us to rewrite this as

$$= \sum_{t=1}^T \mathbb{E}_{p(h_t|\pi)} [H[p(\theta|h_{t-1})] - H[p(\theta|h_t)]] \quad (28)$$

$$= \sum_{t=1}^T \mathbb{E}_{p(h_T|\pi)} [H[p(\theta|h_{t-1})] - H[p(\theta|h_t)]] \quad (29)$$

$$= \mathbb{E}_{p(h_T|\pi)} \left[\sum_{t=1}^T H[p(\theta|h_{t-1})] - H[p(\theta|h_t)] \right] \quad (30)$$

$$= \mathbb{E}_{p(h_T|\pi)} [H[p(\theta)] - H[p(\theta|h_T)]] \quad (31)$$

where the last line follows from the fact that we have a telescopic sum. To complete the proof, we rearrange this as

$$= \mathbb{E}_{p(\theta, h_T | \pi)} [\log p(\theta | h_T) - \log p(\theta)] \quad (32)$$

$$= \mathbb{E}_{p(\theta)p(h_T | \theta, \pi)} \left[\log \frac{p(\theta)p(h_T | \theta, \pi)}{p(h_T | \pi)} - \log p(\theta) \right] \quad (33)$$

$$= \mathbb{E}_{p(\theta)p(h_T | \theta, \pi)} [\log p(h_T | \theta, \pi) - \log p(h_T | \pi)] \quad (34)$$

as required. \square

Theorem 2 (Sequential PCE). *For a design function π and a number of contrastive samples $L \geq 0$, let*

$$\mathcal{L}_T(\pi, L) = \mathbb{E} \left[\log \frac{p(h_T | \theta_0, \pi)}{\frac{1}{L+1} \sum_{\ell=0}^L p(h_T | \theta_\ell, \pi)} \right] \quad (11)$$

where the expectation is over $\theta_0, h_T \sim p(\theta, h_T | \pi)$ and $\theta_{1:L} \sim p(\theta)$ independently. Given minor technical assumptions discussed in the proof, we have³

$$\mathcal{L}_T(\pi, L) \uparrow \mathcal{I}_T(\pi) \text{ as } L \rightarrow \infty \quad (12)$$

at a rate $\mathcal{O}(L^{-1})$.

Proof. We first show that $\mathcal{L}_T(\pi, L)$ is a lower bound to $\mathcal{I}_T(\pi)$:

$$\mathcal{I}_T(\pi) - \mathcal{L}_T(\pi, L) = \mathbb{E}_{p(\theta_0, h_T | \pi)} \left[\log \frac{p(h_T | \theta_0, \pi)}{p(h_T | \pi)} \right] - \mathbb{E}_{p(\theta_0, h_T | \pi)} \mathbb{E}_{p(\theta_{1:L})} \left[\log \frac{p(h_T | \theta_0, \pi)}{\frac{1}{L+1} \sum_{\ell=0}^L p(h_T | \theta_\ell, \pi)} \right] \quad (35)$$

$$= \mathbb{E}_{p(\theta_0, h_T | \pi)} \mathbb{E}_{p(\theta_{1:L})} \left[\log \frac{\frac{1}{L+1} \sum_{\ell=0}^L p(h_T | \theta_\ell, \pi)}{p(h_T | \pi)} \right] \quad (36)$$

$$= \mathbb{E}_{p(\theta_0, h_T | \pi)} \mathbb{E}_{p(\theta_{1:L})} \left[\log \left(\frac{1}{L+1} \sum_{\ell=0}^L \frac{p(\theta_\ell | h_T)}{p(\theta_\ell)} \right) \right] \quad (37)$$

now introducing the shorthand $p(\theta_{0:L}^{-\ell}) := p(\theta_{0:L} \setminus \theta_\ell) = \prod_{j=0, j \neq \ell}^L p(\theta_j)$,

$$= \mathbb{E}_{p(\theta_0, h_T | \pi)} \mathbb{E}_{p(\theta_{1:L})} \left[\log \frac{\frac{1}{L+1} \sum_{\ell=0}^L p(\theta_\ell | h_T) p(\theta_{0:L}^{-\ell})}{p(\theta_{0:L})} \right]. \quad (38)$$

Now by the systemtry on term in side the log, we see that this expectation would be the same if it were instead taken over $p(\theta_i, h_T | \pi) p(\theta_{0:L}^{-i})$ for any $i \in \{0, \dots, L\}$ (with $i = 0$ giving the original form). Furthermore, the result is unchanged if we take the expectation over the mixture distribution $\frac{1}{L+1} \sum_{i=0}^L p(\theta_i, h_T | \pi) p(\theta_{0:L}^{-i}) = p(h_T | \pi) \frac{1}{L+1} \sum_{i=0}^L p(\theta_i | h_T) p(\theta_{0:L}^{-i})$ and thus we have

$$= \mathbb{E}_{p(h_T | \pi)} \mathbb{E}_{\frac{1}{L+1} \sum_{i=0}^L p(\theta_i | h_T) p(\theta_{0:L}^{-i})} \left[\log \frac{\frac{1}{L+1} \sum_{\ell=0}^L p(\theta_\ell | h_T) p(\theta_{0:L}^{-\ell})}{p(\theta_{0:L})} \right] \quad (39)$$

$$= \mathbb{E}_{p(h_T | \pi)} [\text{KL}(\tilde{p}(\theta_{0:L} | h_T) || p(\theta_{0:L}))] \quad (40)$$

where $\tilde{p}(\theta_{0:L} | h_T) = \frac{1}{L+1} \sum_{\ell=0}^L p(\theta_\ell | h_T) p(\theta_{0:L}^{-\ell})$, which is indeed a distribution since

$$\int \tilde{p}(\theta_{0:L} | h_T) d\theta_{0:L} = \frac{1}{L+1} \sum_{\ell=0}^L \left(\int p(\theta_\ell | h_T) d\theta_\ell \cdot \int p(\theta_{0:L}^{-\ell}) d\theta_{0:L} \right) = 1. \quad (41)$$

³ $x_L \uparrow x$ means that x_L is a monotonically increasing sequence in L with limit x .

Now by Gibbs' inequality the expected KL in (40) must be strictly non-negative, establishing $\mathcal{I}_T(\pi) - \mathcal{L}_T(\pi, L) \geq 0$ and thus $\mathcal{I}_T(\pi) \geq \mathcal{L}_T(\pi, L)$ as required.

We next show monotonicity in L , i.e. $\mathcal{L}_T(\pi, L_2) \geq \mathcal{L}_T(\pi, L_1)$ for $L_2 \geq L_1 \geq 0$, using similar argument as above

$$\mathcal{L}_T(\pi, L_2) - \mathcal{L}_T(\pi, L_1) = \mathbb{E}_{p(\theta_0, h_T | \pi)} \mathbb{E}_{p(\theta_{1:L_2})} \left[\log \frac{\frac{1}{L_1+1} \sum_{i=0}^{L_1} p(h_T | \theta_i, \pi)}{\frac{1}{L_2+1} \sum_{j=0}^{L_2} p(h_T | \theta_j, \pi)} \right] \quad (42)$$

$$= \mathbb{E}_{p(\theta_0, h_T | \pi)} \mathbb{E}_{p(\theta_{1:L_2})} \left[\log \frac{\frac{1}{L_1+1} \sum_{i=0}^{L_1} (p(\theta_i | h_T) / p(\theta_i))}{\frac{1}{L_2+1} \sum_{j=0}^{L_2} (p(\theta_j | h_T) / p(\theta_j))} \right] \quad (43)$$

$$= \mathbb{E}_{p(\theta_0, h_T | \pi)} \mathbb{E}_{p(\theta_{1:L_2})} \left[\log \frac{\frac{1}{L_1+1} \sum_{i=0}^{L_1} (p(\theta_i | h_T) p(\theta_{0:L_1}^{-i})) / p(\theta_{0:L_1})}{\frac{1}{L_2+1} \sum_{j=0}^{L_2} (p(\theta_j | h_T) p(\theta_{0:L_2}^{-j})) / p(\theta_{0:L_2})} \right] \quad (44)$$

$$= \mathbb{E}_{p(\theta_0, h_T | \pi)} \mathbb{E}_{p(\theta_{1:L_2})} \left[\log \frac{\frac{1}{L_1+1} \sum_{i=0}^{L_1} p(\theta_i | h_T) p(\theta_{0:L_2}^{-i})}{\frac{1}{L_2+1} \sum_{j=0}^{L_2} p(\theta_j | h_T) p(\theta_{0:L_2}^{-j})} \right] \quad (45)$$

$$= \mathbb{E}_{p(h_T | \pi)} \mathbb{E}_{\frac{1}{L_1+1} \sum_{i=0}^{L_1} p(\theta_i | h_T) p(\theta_{0:L_2}^{-i})} \left[\log \frac{\frac{1}{L_1+1} \sum_{i=0}^{L_1} p(\theta_i | h_T) p(\theta_{0:L_2}^{-i})}{\frac{1}{L_2+1} \sum_{j=0}^{L_2} p(\theta_j | h_T) p(\theta_{0:L_2}^{-j})} \right] \quad (46)$$

$$= \mathbb{E}_{p(h_T | \pi)} [\mathbf{KL}(\tilde{p}_1 || \tilde{p}_2)] \geq 0 \quad (47)$$

where \tilde{p}_1 and \tilde{p}_2 are, respectively, the distributions in the numerator and denominator in (46). The result then again follows by Gibbs' inequality.

Next we show $\mathcal{L}_T(\pi, L) \rightarrow \mathcal{I}_T(\pi)$ as $L \rightarrow \infty$. First, note that the denominator in (11), $\frac{1}{L+1} \sum_{\ell=0}^L p(h_T | \theta_\ell, \pi)$, is a consistent estimator of the marginal $p(h_T | \pi)$, since $\frac{1}{L+1} p(h_T | \theta_0, \pi) \rightarrow 0$, and by the Strong Law of Large Numbers

$$\frac{1}{L+1} \sum_{\ell=1}^L p(h_T | \theta_\ell, \pi) = \frac{L}{L+1} \cdot \frac{1}{L} \sum_{\ell=1}^L p(h_T | \theta_\ell, \pi) \xrightarrow{\text{a.s.}} \mathbb{E}_{p(\theta)} [p(h_T | \theta, \pi)] = p(h_T | \pi). \quad (48)$$

Now from (36) we also have that

$$\mathcal{I}_T(\pi) - \mathcal{L}_T(\pi, L) = \mathbb{E}_{p(\theta_0, h_T | \pi)} \mathbb{E}_{p(\theta_{1:L})} \left[\log \frac{\frac{1}{L+1} \sum_{\ell=0}^L p(h_T | \theta_\ell, \pi)}{p(h_T | \pi)} \right] \quad (49)$$

and we have $\log \frac{\frac{1}{L+1} \sum_{\ell=0}^L p(h_T | \theta_\ell, \pi)}{p(h_T | \pi)} \rightarrow 0$ almost surely as $L \rightarrow \infty$. The minor technical assumption, which is required to establish convergence is that there exist some $0 < \kappa_1, \kappa_2 < \infty$ such that⁴

$$\kappa_1 \leq \frac{p(h_T | \theta, \pi)}{p(h_T | \pi)} \leq \kappa_2 \quad \forall \theta, h_T. \quad (50)$$

using this assumption, the integrand of (49) is bounded, because

$$\left| \log \frac{\frac{1}{L+1} \sum_{\ell=0}^L p(h_T | \theta_\ell, \pi)}{p(h_T | \pi)} \right| = \left| \log \left(\frac{1}{L+1} \sum_{\ell=0}^L \frac{p(h_T | \theta_\ell, \pi)}{p(h_T | \pi)} \right) \right| \quad (51)$$

$$\leq \max \left(\left| \log \left(\max_{\ell} \frac{p(h_T | \theta_\ell, \pi)}{p(h_T | \pi)} \right) \right|, \left| \log \left(\min_{\ell} \frac{p(h_T | \theta_\ell, \pi)}{p(h_T | \pi)} \right) \right| \right) \quad (52)$$

$$\leq \max (|\log \kappa_2|, |\log \kappa_1|) \quad (53)$$

$$< \infty. \quad (54)$$

⁴In practice, we can actually weaken this assumption significantly if necessary by making κ_1 and κ_2 dependent on h_T and θ then assuming that the expectation $\mathbb{E}_{p(\theta_0, h_T | \pi)} \mathbb{E}_{p(\theta_{1:L})} [\log |\kappa_i(\theta_j, h_T)|]$ is finite for $i \in \{1, 2\}$ and $j \in \{0, 1\}$. This then permits $\kappa_1(h_T, \theta) \rightarrow 0$ and $\kappa_2(h_T, \theta) \rightarrow \infty$ for certain h_T and θ , provided that these events are zero measure under both $p(\theta, h_T | \pi)$ and $p(\theta) p(h_T | \pi)$, thereby avoiding potential issues with tail behavior in the limits of extreme values for θ .

Thus, the Bounded Convergence Theorem can be applied to conclude that $\mathcal{I}_T(\pi) - \mathcal{L}_T(\pi, L) \rightarrow 0$ as $L \rightarrow \infty$.

Finally, for the rate of convergence we apply the inequality $\log x \leq x - 1$ to (36) to get

$$\mathcal{I}_T(\pi) - \mathcal{L}_T(\pi, L) = \mathbb{E}_{p(\theta_0, h_T | \pi)} \mathbb{E}_{p(\theta_{1:L})} \left[\log \frac{\frac{1}{L+1} \sum_{\ell=0}^L p(h_T | \theta_\ell, \pi)}{p(h_T | \pi)} \right] \quad (55)$$

$$\leq \mathbb{E}_{p(\theta_0, h_T | \pi)} \mathbb{E}_{p(\theta_{1:L})} \left[\frac{\frac{1}{L+1} \sum_{\ell=0}^L p(h_T | \theta_\ell, \pi)}{p(h_T | \pi)} - 1 \right] \quad (56)$$

$$= \mathbb{E}_{p(\theta_0, h_T | \pi)} \left[\frac{\frac{1}{L+1} \left(p(h_T | \theta_0 \pi) + \sum_{\ell=1}^L \mathbb{E}_{p(\theta_{1:L})} [p(h_T | \theta_\ell, \pi)] \right)}{p(h_T | \pi)} - 1 \right] \quad (57)$$

$$= \mathbb{E}_{p(\theta_0, h_T | \pi)} \left[\frac{\frac{1}{L+1} (p(h_T | \theta_0 \pi) + L p(h_T | \pi))}{p(h_T | \pi)} - 1 \right] \quad (58)$$

$$= \frac{1}{L+1} \mathbb{E}_{p(\theta_0, h_T | \pi)} \left[\frac{p(h_T | \theta_0, \pi)}{p(h_T | \pi)} - 1 \right] \quad (59)$$

$$= \frac{C}{L+1}, \quad (60)$$

where we can conclude $C < \infty$ using (50). Combining this with our previous result showing that $\mathcal{L}_T(\pi, L)$ is a lower bound on $\mathcal{I}_T(\pi)$, we have shown that

$$0 \leq \mathcal{I}_T(\pi) - \mathcal{L}_T(\pi, L) \leq \frac{C}{L+1}. \quad (61)$$

This establishes the $\mathcal{O}(L^{-1})$ rate of convergence. \square

Theorem 3 (Permutation invariance). *Consider a permutation $\sigma \in S_k$ acting on a history h_k^1 , yielding $h_k^2 = (\xi_{\sigma(1)}, y_{\sigma(1)}), \dots, (\xi_{\sigma(k)}, y_{\sigma(k)})$. For all such σ , we have*

$$\mathbb{E} \left[\sum_{t=1}^T I_{h_{t-1}}(\xi_t) \middle| h_k = h_k^1 \right] = \mathbb{E} \left[\sum_{t=1}^T I_{h_{t-1}}(\xi_t) \middle| h_k = h_k^2 \right]$$

showing that the EIG is unchanged under permutation. Further, the optimal policies starting in h_k^1 and h_k^2 are the same.

Technical note: In this statement, the first expectation is with respect to $p(h_T | \pi)$ for policy π and the second is with respect to $p(h_T | \pi')$, where for $t > k$ we set $\pi'(h_t) = \pi(\sigma^{-1}(h_t))$ where σ^{-1} acts on the first k labels by permutation and as the identity on other labels. This means we remove *explicit* variability under permutation caused by π , and show that no other source of variability can arise.

Proof. To begin, we set up some notation. Given the partial history $h_k = h_k^1$, we complete the experiment by sampling (ξ_t, y_t) for $t = k+1, \dots, T$. We denote the resulting full history as h_T^1 , and define h_T^2 similarly. Next, we use Theorem 1 to rewrite the conditional objective under consideration as

$$\mathbb{E}_{p(h_T^1 | \pi)} \left[\sum_{t=1}^T I_{h_{t-1}}(\xi_t) \middle| h_k = h_k^1 \right] = \mathbb{E}_{p(\theta | h_k^1)} \prod_{t=k+1}^T p(y_t | \theta, \xi_t) [\log p(h_T^1 | \theta, \pi) - \log p(h_T^1 | \pi)] \quad (62)$$

$$= \mathbb{E}_{p(\theta | h_k^1)} \prod_{t=k+1}^T p(y_t | \theta, \xi_t) [\log p(\theta | h_T^1) - \log p(\theta)] \quad (63)$$

$$= \mathbb{E}_{p(\theta | h_k^1) p(h_T^1 | h_k^1, \theta, \pi)} [\log p(\theta | h_T^1) - \log p(\theta)]. \quad (64)$$

A central point of the proof is that the posterior distribution $p(\theta | h_t)$ is invariant to the order of the history. Indeed, we have

$$p(\theta | h_t) \propto p(\theta) \prod_{s=1}^t p(y_s | \theta, \xi_s) \quad (65)$$

which shows that $p(\theta|h_k^1) = p(\theta|h_k^2)$. Given a continuation of the history $(\xi_{k+1}, y_{k+1}), \dots, (\xi_T, y_T)$, if we use the same continuation starting from h_k^1 and h_k^2 to give h_T^1 and h_T^2 then we have $p(\theta|h_T^1) = p(\theta|h_T^2)$. However, we need to show that the continuations $(\xi_{k+1}, y_{k+1}), \dots, (\xi_T, y_T)$ are equal in distribution.

We now show that the sampling distributions of $(\xi_{k+1}, y_{k+1}), \dots, (\xi_T, y_T)$ are equal starting from h_k^1 and h_k^2 . We have shown that $\theta \sim p(\theta|h_k^1)$ is unchanged in distribution if we instead sample $\theta \sim p(\theta|h_k^2)$. Further, we have

$$\xi_{k+1}^1 = \pi(h_k^1) \quad \xi_{k+1}^2 = \pi'(h_k^2) \quad (66)$$

which, by the construction of π' implies $\xi_{k+1}^1 = \xi_{k+1}^2$. Together, these results imply that the observations y_{k+1}^1 and y_{k+1}^2 are equal in distribution. Proceeding inductively, since h_{k+1}^1 and h_{k+1}^2 are equal in distribution a similar argument shows that h_{k+2}^1 and h_{k+2}^2 have the same distribution. Continuing in this way, we have that h_T^1 and h_T^2 are equal in distribution. Together, these results imply that

$$\mathbb{E}_{p(\theta|h_k^1)p(h_T^1|h_k^1, \theta, \pi)} [\log p(\theta|h_T^1) - \log p(\theta)] = \mathbb{E}_{p(\theta|h_k^2)p(h_T^2|h_k^2, \theta, \pi')} [\log p(\theta|h_T^2) - \log p(\theta)] \quad (67)$$

which conclude the first part of the proof.

To establish the permutation invariance of the optimal policy π^* , we reason by induction starting with $k = T - 1$, using a dynamic programming style argument. Given h_{T-1} , the total EIG is a function of $p(\theta|h_{T-1})$ and ξ_T . Since we do not need to account for future asymmetry in the policy, we immediately have that the optimal final design ξ_T only depends on $p(\theta|h_{T-1})$, which implies that is invariant to the order of the history.

We now assume that the optimal policy is permutation invariant starting from $k + 2$. Using the previous result (67), we separate out the design ξ_{k+1} and substitute π^* for both π and π' (since it is permutation invariant for the steps after $k + 1$ by inductive hypothesis) to give

$$\begin{aligned} & \mathbb{E}_{p(\theta|h_k^1)p(y_{k+1}|\theta, \xi_{k+1}) \prod_{t=k+2}^T p(y_t|\theta, \pi^*(h_{t-1}))} [\log p(\theta|h_T^1) - \log p(\theta)] \\ &= \mathbb{E}_{p(\theta|h_k^2)p(y_{k+1}|\theta, \xi_{k+1}) \prod_{t=k+2}^T p(y_t|\theta, \pi^*(h_{t-1}))} [\log p(\theta|h_T^2) - \log p(\theta)]. \end{aligned} \quad (68)$$

To extend the optimal policy to $k + 1$, we consider choosing ξ_{k+1} and then following π^* thereafter. As (68) shows us, the decision problem for ξ_{k+1} is the same starting from h_k^1 and h_k^2 because the posterior distributions $p(\theta|h_k^1)$ and $p(\theta|h_k^2)$ are equal, and the optimal policy after $k + 1$ does not depend on history order. This implies that the optimal choice of ξ_{k+1} is the same for h_k^1 and h_k^2 . This implies that the optimal policies starting in h_k^1 and h_k^2 are the same. This completes the proof. \square

Theorem 4. For a design function π and a number of contrastive samples $L \geq 1$, let

$$\mathcal{U}_T(\pi, L) = \mathbb{E} \left[\log \frac{p(h_T|\theta_0, \pi)}{\frac{1}{L} \sum_{\ell=1}^L p(h_T|\theta_\ell, \pi)} \right] \quad (69)$$

where the expectation is over $\theta_0, h_T \sim p(\theta, h_T|\pi)$ and $\theta_{1:L} \sim p(\theta)$ independently. Then,

$$\mathcal{U}_T(\pi, L) \downarrow \mathcal{I}_T(\pi) \text{ as } L \rightarrow \infty \quad (70)$$

at a rate $\mathcal{O}(L^{-1})$.

Proof. We first show $\mathcal{U}_T(\pi, L)$ is an upper bound to $\mathcal{I}_T(\pi)$

$$\mathcal{U}_T(\pi, L) - \mathcal{I}_T(\pi) = \mathbb{E}_{p(\theta_0, h_T|\pi)} \mathbb{E}_{p(\theta_{1:L})} \left[\log \frac{p(h_T|\theta_0, \pi)}{\frac{1}{L} \sum_{\ell=1}^L p(h_T|\theta_\ell, \pi)} \right] - \mathbb{E}_{p(\theta_0, h_T|\pi)} \left[\log \frac{p(h_T|\theta_0, \pi)}{p(h_T|\pi)} \right] \quad (71)$$

$$= \mathbb{E}_{p(\theta_0, h_T|\pi)} \mathbb{E}_{p(\theta_{1:L})} \left[\log p(h_T|\pi) - \log \left(\frac{1}{L} \sum_{\ell=1}^L p(h_T|\theta_\ell, \pi) \right) \right] \quad (72)$$

now using Jensen's inequality

$$\geq \mathbb{E}_{p(\theta_0, h_T|\pi)} \left[\log p(h_T|\pi) - \log \left(\frac{1}{L} \sum_{\ell=1}^L \mathbb{E}_{p(\theta_\ell)} [p(h_T|\theta_\ell, \pi)] \right) \right] \quad (73)$$

$$= \mathbb{E}_{p(\theta_0, h_T|\pi)} \left[\log p(h_T|\pi) - \log \left(\frac{1}{L} \sum_{\ell=1}^L p(h_T|\pi) \right) \right] \quad (74)$$

$$= \mathbb{E}_{p(\theta_0, h_T|\pi)} [\log p(h_T|\pi) - \log p(h_T|\pi)] \quad (75)$$

$$= 0. \quad (76)$$

To show monotonicity in L , pick $L_2 \geq L_1 \geq 0$ and consider the difference

$$\delta := \mathcal{U}_T(\pi, L_1) - \mathcal{U}_T(\pi, L_2) = \mathbb{E}_{p(\theta_0, h_T|\pi)} \mathbb{E}_{p(\theta_{1:L_2})} \left[\log \frac{\frac{1}{L_2} \sum_{j=1}^{L_2} p(h_T|\theta_j, \pi)}{\frac{1}{L_1} \sum_{i=1}^{L_1} p(h_T|\theta_i, \pi)} \right]. \quad (77)$$

Notice that we can write expression in the numerator $\frac{1}{L_2} \sum_{j=1}^{L_2} p(h_T|\theta_j, \pi) = \mathbb{E}_{J_1, \dots, J_{L_1}} \left[\frac{1}{L_1} \sum_{k=1}^{L_1} p(h_T|\theta_{J_k}, \pi) \right]$, where the indices J_k have been uniformly drawn from $1, \dots, L_2$. We have

$$\delta = \mathbb{E}_{p(\theta_0, h_T|\pi)} \mathbb{E}_{p(\theta_{1:L_2})} \left[\log \mathbb{E}_{J_1, \dots, J_{L_1}} \left[\frac{1}{L_1} \sum_{k=1}^{L_1} p(h_T|\theta_{J_k}, \pi) \right] - \log \frac{1}{L_1} \sum_{i=1}^{L_1} p(h_T|\theta_i, \pi) \right] \quad (78)$$

now applying Jensen's Inequality

$$\geq \mathbb{E}_{p(\theta_0, h_T|\pi)} \mathbb{E}_{p(\theta_{1:L_2})} \left[\mathbb{E}_{J_1, \dots, J_{L_1}} \left[\log \frac{1}{L_1} \sum_{k=1}^{L_1} p(h_T|\theta_{J_k}, \pi) \right] - \log \frac{1}{L_1} \sum_{i=1}^{L_1} p(h_T|\theta_i, \pi) \right] \quad (79)$$

then use the fact that any L_1 -subset of $\theta_1, \dots, \theta_{L_2}$ has the same distribution

$$= \mathbb{E}_{p(\theta_0, h_T|\pi)} \mathbb{E}_{p(\theta_{1:L_2})} \left[\log \frac{1}{L_1} \sum_{i=1}^{L_1} p(h_T|\theta_i, \pi) - \log \frac{1}{L_1} \sum_{i=1}^{L_1} p(h_T|\theta_i, \pi) \right] = 0 \quad (80)$$

which establishes monotonicity.

Finally, convergence is shown analogously to Theorem 2. Again we adopt the assumption (50). The Strong Law of Large Numbers gives us almost sure convergence $\log \left(\frac{1}{L} \sum_{\ell=1}^L p(h_T|\theta_\ell, \pi) \right) \rightarrow \log p(h_T|\pi)$ as $L \rightarrow \infty$. Applying the Bounded Convergence Theorem, as in Theorem 2, we have

$$\lim_{L \rightarrow \infty} (\mathcal{U}_T(\pi, L) - \mathcal{I}_T(\pi, L)) = \mathbb{E}_{p(\theta_0, h_T|\pi)} \mathbb{E}_{p(\theta_{1:L})} \left[\lim_{L \rightarrow \infty} \log \frac{p(h_T|\pi)}{\frac{1}{L} \sum_{\ell=1}^L p(h_T|\theta_\ell, \pi)} \right] \quad (81)$$

$$= 0. \quad (82)$$

Finally, for the rate of convergence, we have

$$\mathcal{U}_T(\pi, L) - \mathcal{I}_T(\pi) = \mathbb{E}_{p(\theta_0, h_T|\pi)} \mathbb{E}_{p(\theta_{1:L})} \left[\log \frac{p(h_T|\pi)}{\frac{1}{L} \sum_{\ell=1}^L p(h_T|\theta_\ell, \pi)} \right] \quad (83)$$

$$= \mathbb{E}_{p(\theta_0, h_T|\pi)} \mathbb{E}_{p(\theta_{1:L})} \left[-\log \left(\frac{1}{L} \sum_{\ell=1}^L \frac{p(h_T|\theta_\ell, \pi)}{p(h_T|\pi)} \right) \right] \quad (84)$$

$$= \mathbb{E}_{p(\theta_0, h_T|\pi)} \mathbb{E}_{p(\theta_{1:L})} \left[-\log \left(1 + \frac{1}{L} \sum_{\ell=1}^L \left(\frac{p(h_T|\theta_\ell, \pi)}{p(h_T|\pi)} - 1 \right) \right) \right] \quad (85)$$

$$= \mathbb{E}_{p(\theta_0, h_T|\pi)} \mathbb{E}_{p(\theta_{1:L})} \left[\sum_{n=1}^{\infty} (-1)^n \frac{x^n}{n} \right] \quad (86)$$

where $x = \frac{1}{L} \sum_{\ell=1}^L \left(\frac{p(h_T|\theta_\ell, \pi)}{p(h_T|\pi)} - 1 \right)$ and we have applied the Taylor expansion for $\log(1+x)$. We have

$$\mathbb{E}_{p(\theta_0, h_T|\pi)} \mathbb{E}_{p(\theta_{1:L})} [x] = 0 \quad (87)$$

$$\mathbb{E}_{p(\theta_0, h_T|\pi)} \mathbb{E}_{p(\theta_{1:L})} [x^2] = \frac{1}{L} \mathbb{E}_{p(\theta_0, h_T|\pi)} \mathbb{E}_{p(\theta_{1:L})} \left[\left(\frac{p(h_T|\theta_\ell, \pi)}{p(h_T|\pi)} - 1 \right)^2 \right] \quad (88)$$

and higher order terms are $o(L^{-1})$ (Angelova, 2012; Nowozin, 2018). This shows that $\mathcal{U}_T(\pi, L) - \mathcal{I}_T(\pi) \rightarrow 0$ at a rate $\mathcal{O}(L^{-1})$. This concludes the proof. \square

B. Additional bounds

In this section, we consider a parametrized proposal distribution $q(\theta; h_T)$ which can be used to approximate the posterior $p(\theta|h_T)$. One example of such a proposal would be an amortized variational approximation to the posterior that takes as input h_T and outputs a variational distribution over θ . It would be possible to share the representation $R(h_T)$ from (18) between the design network and the inference network. However, the following theorem is not limited to variational posteriors, and concerns any parametrized proposal distribution.

Theorem 5. *For a design function π , a number of contrastive samples $L \geq 1$, and a parametrized proposal $q(\theta; h_T)$, we have the sequential Adaptive Contrastive Estimation (sACE) lower bound*

$$\mathcal{I}_T(\pi) \geq \mathbb{E}_{p(\theta_0, h_T|\pi)q(\theta_{1:L}; h_T)} \left[\log \frac{p(h_T|\theta_0, \pi)}{\frac{1}{L+1} \sum_{\ell=0}^L \frac{p(h_T|\theta_\ell, \pi)p(\theta_\ell)}{q(\theta_\ell; h_T)}} \right] \quad (89)$$

and the sequential Variational Nested Monte Carlo (sVNMC) upper bound

$$\mathcal{I}_T(\pi) \leq \mathbb{E}_{p(\theta_0, h_T|\pi)q(\theta_{1:L}; h_T)} \left[\log \frac{p(h_T|\theta_0, \pi)}{\frac{1}{L} \sum_{\ell=1}^L \frac{p(h_T|\theta_\ell, \pi)p(\theta_\ell)}{q(\theta_\ell; h_T)}} \right]. \quad (90)$$

Proof. We begin by showing the sACE lower bound. The proof closely follows that of Theorem 2. We have the error term

$$\delta_{sACE} = \mathbb{E}_{p(\theta_0, h_T|\pi)} \left[\log \frac{p(h_T|\theta_0, \pi)}{p(h_T|\pi)} \right] - \mathbb{E}_{p(\theta_0, h_T|\pi)} \mathbb{E}_{q(\theta_{1:L}; h_T)} \left[\log \frac{p(h_T|\theta_0, \pi)}{\frac{1}{L+1} \sum_{\ell=0}^L \frac{p(h_T|\theta_\ell, \pi)p(\theta_\ell)}{q(\theta_\ell; h_T)}} \right] \quad (91)$$

$$= \mathbb{E}_{p(\theta_0, h_T|\pi)} \mathbb{E}_{q(\theta_{1:L}; h_T)} \left[\log \frac{\frac{1}{L+1} \sum_{\ell=0}^L \frac{p(h_T|\theta_\ell, \pi)p(\theta_\ell)}{q(\theta_\ell; h_T)}}{p(h_T|\pi)} \right] \quad (92)$$

$$= \mathbb{E}_{p(\theta_0, h_T|\pi)} \mathbb{E}_{q(\theta_{1:L}; h_T)} \left[\log \left(\frac{1}{L+1} \sum_{\ell=0}^L \frac{p(\theta_\ell|h_T)}{q(\theta_\ell; h_T)} \right) \right] \quad (93)$$

now introducing the shorthand $q(\theta_{0:L}^{-\ell}; h_T) := q(\theta_{0:L} \setminus \theta_\ell; h_T) = \prod_{j=0, j \neq \ell}^L q(\theta_j; h_T)$,

$$= \mathbb{E}_{p(\theta_0, h_T|\pi)} \mathbb{E}_{q(\theta_{1:L}; h_T)} \left[\log \frac{\frac{1}{L+1} \sum_{\ell=0}^L p(\theta_\ell|h_T)q(\theta_{0:L}^{-\ell}; h_T)}{q(\theta_{0:L}; h_T)} \right]. \quad (94)$$

Now by the symmetry on term in side the log, we see that this expectation would be the same if it were instead taken over $p(\theta_i, h_T|\pi)q(\theta_{0:L}^{-i}; h_T)$ for any $i \in \{0, \dots, L\}$. It is also the same if we take the expectation over $\frac{1}{L+1} \sum_{i=0}^L p(\theta_i, h_T|\pi)q(\theta_{0:L}^{-i}; h_T) = p(h_T|\pi) \frac{1}{L+1} \sum_{i=0}^L p(\theta_i|h_T)q(\theta_{0:L}^{-i}; h_T)$ and thus we have

$$= \mathbb{E}_{p(h_T|\pi)} \mathbb{E}_{\frac{1}{L+1} \sum_{i=0}^L p(\theta_i|h_T)q(\theta_{0:L}^{-i}; h_T)} \left[\log \frac{\frac{1}{L+1} \sum_{\ell=0}^L p(\theta_\ell|h_T)q(\theta_{0:L}^{-\ell}; h_T)}{q(\theta_{0:L}; h_T)} \right] \quad (95)$$

$$= \mathbb{E}_{p(h_T|\pi)} [\text{KL}(\check{q}(\theta_{0:L}; h_T) || q(\theta_{0:L}; h_T))] \quad (96)$$

where $\check{q}(\theta_{0:L}; h_T) = \frac{1}{L+1} \sum_{\ell=0}^L p(\theta_\ell | h_T) q(\theta_{0:L}^{-\ell}; h_T)$, which is indeed a distribution since

$$\int \check{q}(\theta_{0:L}; h_T) d\theta_{0:L} = \frac{1}{L+1} \sum_{\ell=0}^L \left(\int p(\theta_\ell | h_T) d\theta_\ell \cdot \int q(\theta_{0:L}^{-\ell}; h_T) d\theta_{0:L}^{-\ell} \right) = 1. \quad (97)$$

Now by Gibb's inequality the expected KL in (96) must be strictly non-negative, establishing the required lower bound.

Turning to the sVNMCMC bound, we use a proof that is close in spirit to Theorem 4. We have the error term

$$\delta_{sVNMCMC} = \mathbb{E}_{p(\theta_0, h_T | \pi)} \mathbb{E}_{q(\theta_{1:L}; h_T)} \left[\log \frac{p(h_T | \theta_0, \pi)}{\frac{1}{L} \sum_{\ell=1}^L \frac{p(h_T | \theta_\ell, \pi) p(\theta_\ell)}{q(\theta_\ell; h_T)}} \right] - \mathbb{E}_{p(\theta_0, h_T | \pi)} \left[\log \frac{p(h_T | \theta_0, \pi)}{p(h_T | \pi)} \right] \quad (98)$$

$$= \mathbb{E}_{p(\theta_0, h_T | \pi)} \mathbb{E}_{q(\theta_{1:L}; h_T)} \left[\log p(h_T | \pi) - \log \left(\frac{1}{L} \sum_{\ell=1}^L \frac{p(h_T | \theta_\ell, \pi) p(\theta_\ell)}{q(\theta_\ell; h_T)} \right) \right] \quad (99)$$

now using Jensen's inequality

$$\geq \mathbb{E}_{p(\theta_0, h_T | \pi)} \left[\log p(h_T | \pi) - \log \left(\frac{1}{L} \sum_{\ell=1}^L \mathbb{E}_{q(\theta_\ell; h_T)} \left[\frac{p(h_T | \theta_\ell, \pi) p(\theta_\ell)}{q(\theta_\ell; h_T)} \right] \right) \right] \quad (100)$$

$$= \mathbb{E}_{p(\theta_0, h_T | \pi)} \left[\log p(h_T | \pi) - \log \left(\frac{1}{L} \sum_{\ell=1}^L \mathbb{E}_{p(\theta_\ell)} [p(h_T | \theta_\ell, \pi)] \right) \right] \quad (101)$$

$$= \mathbb{E}_{p(\theta_0, h_T | \pi)} \left[\log p(h_T | \pi) - \log \left(\frac{1}{L} \sum_{\ell=1}^L p(h_T | \pi) \right) \right] \quad (102)$$

$$= \mathbb{E}_{p(\theta_0, h_T | \pi)} [\log p(h_T | \pi) - \log p(h_T | \pi)] \quad (103)$$

$$= 0. \quad (104)$$

This establishes the upper bound. \square

C. Gradient details

We begin by presenting a derivation of the gradient (16). Initially, we provide a more complete description of our notation. Suppose ξ the design is of dimension D_1 and y the observation is of dimension D_2 . Then $u = (\xi, y)$ is of dimension $D_1 + D_2$. For an arbitrary scalar quantity x , we have

$$\frac{\partial x}{\partial u} = \left(\frac{\partial x}{\partial \xi^{(1)}} \quad \cdots \quad \frac{\partial x}{\partial \xi^{(D_1)}} \quad \frac{\partial x}{\partial y^{(1)}} \quad \cdots \quad \frac{\partial x}{\partial y^{(D_2)}} \right) \quad (105)$$

and

$$\frac{\partial u}{\partial x} = \left(\frac{\partial \xi^{(1)}}{\partial x} \quad \cdots \quad \frac{\partial \xi^{(D_1)}}{\partial x} \quad \sum_{d=1}^{D_1} \frac{\partial y^{(1)}}{\partial \xi^{(d)}} \frac{\partial \xi^{(d)}}{\partial x} \quad \cdots \quad \sum_{d=1}^{D_1} \frac{\partial y^{(D_2)}}{\partial \xi^{(d)}} \frac{\partial \xi^{(d)}}{\partial x} \right)^\top. \quad (106)$$

This notation enables us to concisely and clearly deal with both scalar and vector quantities. In general, the derivatives $\partial a / \partial b$ and da / db represent a matrix of shape $(\dim a, \dim b)$ where one or both of a, b may have dimension 1. This notation is particularly attractive because the Chain Rule for partial derivatives can be concisely expressed as follows. Suppose $a = a(b_1(c), \dots, b_n(c), c)$, then the total derivative is given by

$$\frac{da}{dc} = \frac{\partial a}{\partial c} + \sum_{i=1}^n \frac{\partial a}{\partial b_i} \frac{db_i}{dc} \quad (107)$$

where the normal rules of matrix multiplication apply. We now apply this in the context of the function $g(\theta_{0:L}, h_T)$ which was defined in Section 4.2.

We have $g = g(\theta_{0:L}, u_1, \dots, u_T)$. The Chain Rule implies that

$$\frac{dg}{d\phi} = \sum_{t=1}^T \frac{\partial g}{\partial u_t} \frac{du_t}{d\phi}. \quad (108)$$

We also have, for $t = 1, \dots, T$, that $u_t = u(\phi, h_{t-1}, \theta_0, \epsilon_t) = u(\phi, u_1, \dots, u_{t-1}, \theta_0, \epsilon_t)$. This represents the dependence of ξ_t on h_{t-1} via π_ϕ , and the further dependence of y_t on θ_0 and ϵ_t . Expanding the derivatives again using the Chain Rule gives

$$\frac{dg}{d\phi} = \sum_{t=1}^T \frac{\partial g}{\partial u_t} \left(\frac{\partial u_t}{\partial \phi} + \sum_{s=1}^{t-1} \frac{\partial u_t}{\partial u_s} \frac{du_s}{d\phi} \right). \quad (109)$$

Again, we can expand the total derivative to give

$$\frac{dg}{d\phi} = \sum_{t=1}^T \frac{\partial g}{\partial u_t} \left(\frac{\partial u_t}{\partial \phi} + \sum_{s=1}^{t-1} \frac{\partial u_t}{\partial u_s} \left(\frac{\partial u_s}{\partial \phi} + \sum_{r=1}^{s-1} \frac{\partial u_s}{\partial u_r} \frac{du_r}{d\phi} \right) \right). \quad (110)$$

Rather than continuing in this manner, we observe that the current expansion (110) can be split up as follows

$$\frac{dg}{d\phi} = \sum_{t=1}^T \frac{\partial g}{\partial u_t} \frac{\partial u_t}{\partial \phi} + \sum_{1 \leq s < t \leq T} \frac{\partial g}{\partial u_t} \frac{\partial u_t}{\partial u_s} \frac{\partial u_s}{\partial \phi} + \sum_{1 \leq r < s < t \leq T} \frac{\partial g}{\partial u_t} \frac{\partial u_t}{\partial u_s} \frac{\partial u_s}{\partial u_r} \frac{du_r}{d\phi} \quad (111)$$

which shows that we have completely enumerated over all paths of length 1 and 2 through the computational graph, and the final term with a total derivative concerns paths of length 3 or more. This approach can be naturally extended to enumerate over all paths. To write this concisely, we introduce a new variable k which denotes the length of the path, and then a sum over all increasing sequences $1 \leq t_1 < \dots < t_k \leq T$. This gives

$$\frac{dg}{d\phi} = \sum_{k=1}^T \left[\sum_{1 \leq t_1 < \dots < t_k \leq T} \frac{\partial g}{\partial u_{t_k}} \frac{\partial u_{t_k}}{\partial u_{t_{k-1}}} \dots \frac{\partial u_{t_2}}{\partial u_{t_1}} \frac{\partial u_{t_1}}{\partial \phi} \right]. \quad (112)$$

This can be written concisely as

$$\frac{dg}{d\phi} = \sum_{\substack{k \in \{1, \dots, T\} \\ 1 \leq t_1 < \dots < t_k \leq T}} \frac{\partial g}{\partial u_{t_k}} \left(\prod_{j=1}^{k-1} \frac{\partial u_{t_{j+1}}}{\partial u_{t_j}} \right) \frac{\partial u_{t_1}}{\partial \phi} \quad (113)$$

where the product is interpreted in the order given in (112) for the matrix multiplication to operate correctly, and an empty product is equal to the identity. This is exactly (16). In practice, derivatives of this form are calculated automatically in PyTorch (Paszke et al., 2019).

C.1. Discrete observations

We can extend our approach to models in which the observation $y \in \mathcal{Y}$ is a discrete random variable. Given a policy π_ϕ , the only random parts of the history h_T are the observations y_1, \dots, y_T with the designs being computed deterministically from past histories, giving $|\mathcal{Y}|^T$ possible histories for the experiment. A naive approach, then, would be to integrate over all possible values of h_T in the definition of $\mathcal{L}_T(\pi_\phi, L)$ and take gradients with respect to ϕ to give

$$\frac{d\mathcal{L}_T}{d\phi} = \mathbb{E}_{p(\theta_{0:L})} \left[\sum_{h_T} \frac{d p(h_T | \theta_0) g_L(\theta_{0:L}, h_T)}{d\phi} \right] \quad (114)$$

where the sum is over all histories for the current policy π_ϕ . Unfortunately, computing this gradient has a computational cost $\mathcal{O}(|\mathcal{Y}|^T)$, which presents a challenge even for moderate T .

To compute a tractable gradient estimate, we use the same approach as we used in the previous section of considering the partial derivative in place of the total derivative. Expanding using the Chain Rule leads to

$$\mathbb{E}_{p(\theta_{0:L})} \left[\sum_{h_T} \frac{\partial p(h_T | \theta_0) g_L(\theta_{0:L}, h_T)}{\partial \phi} \right] = \mathbb{E}_{p(\theta_{0:L})} \left[\sum_{h_T} \sum_{\tau=1}^T \frac{\partial p(h_T | \theta_0) g_L(\theta_{0:L}, h_T)}{\partial \xi_\tau} \frac{\partial \xi_\tau}{\partial \phi} \right]. \quad (115)$$

At first sight, this does not seem to have led to an improvement as we still have a sum over h_T . However, the following Lemma then shows that we can evaluate (115) by summing over y_τ to compute the ξ_τ gradient, but then taking samples for other $y_s, s \neq \tau$. This results in a computation over $|\mathcal{Y}|$ histories, which when summed over τ , leads to a gradient estimator of computational cost $\mathcal{O}(|\mathcal{Y}|T)$. This is a significant improvement from the total enumeration and provides a suitable training gradient for a range of values of T . The following Lemma makes this precise.

Lemma 6 (Discrete gradient). *The gradient in (115) can be written*

$$\mathbb{E}_{p(\theta_{0:L})} \left[\sum_{h_T} \sum_{\tau=1}^T \frac{\partial p(h_T|\theta_0)g_L(\theta_{0:L}, h_T)}{\partial \xi_\tau} \frac{\partial \xi_\tau}{\partial \phi} \right] = \sum_{\tau=1}^T \mathbb{E}_{p(\theta_{0:L})p(h_{\tau-1}|\theta_0, \pi_\phi)} \left[\sum_{y_\tau} \mathbb{E}_{p(h_T|h_\tau, \theta_0, \pi_\phi)} [a_\tau(h_T)] \right] \quad (116)$$

where

$$a_\tau(h_T) = \frac{\partial p(y_\tau|\theta_0, \xi_\tau)g_L(\theta_{0:L}, h_T)}{\partial \xi_\tau} \frac{\partial \xi_\tau}{\partial \phi}. \quad (117)$$

We can construct an unbiased estimator of (116) by taking a single sample of $h_{\tau-1}$, and then taking $|\mathcal{Y}|$ samples of h_T that share $h_{\tau-1}$ in common and differ in the value of y_τ . This estimator can be computed in $\mathcal{O}(|\mathcal{Y}|T)$.

Proof. We begin by decomposing the gradient using the definition of $p(h_T|\theta_0)$

$$\frac{\partial p(h_T|\theta_0)g_L(\theta_{0:L}, h_T)}{\partial \xi_\tau} \frac{\partial \xi_\tau}{\partial \phi} = \frac{\partial}{\partial \xi_\tau} \left(\left(\prod_{s=1}^T p(y_s|\theta_0, \xi_s) \right) g_L(\theta_{0:L}, h_T) \right) \frac{\partial \xi_\tau}{\partial \phi} \quad (118)$$

$$= \left(\prod_{s \neq \tau} p(y_s|\theta_0, \xi_s) \right) \frac{\partial p(y_\tau|\theta_0, \xi_\tau)g_L(\theta_{0:L}, h_T)}{\partial \xi_\tau} \frac{\partial \xi_\tau}{\partial \phi} \quad (119)$$

$$= \left(\prod_{s \neq \tau} p(y_s|\theta_0, \xi_s) \right) a_\tau(h_T). \quad (120)$$

Substituting this back into the partial derivative gives

$$\begin{aligned} & \mathbb{E}_{p(\theta_{0:L})} \left[\sum_{h_T} \sum_{\tau=1}^T \frac{\partial p(h_T|\theta_0)g_L(\theta_{0:L}, h_T)}{\partial \xi_\tau} \frac{\partial \xi_\tau}{\partial \phi} \right] \\ &= \mathbb{E}_{p(\theta_{0:L})} \left[\sum_{h_T} \sum_{\tau=1}^T \left(\prod_{s \neq \tau} p(y_s|\theta_0, \xi_s) \right) a_\tau(h_T) \right] \end{aligned} \quad (121)$$

$$= \sum_{\tau=1}^T \mathbb{E}_{p(\theta_{0:L})} \left[\sum_{h_T} \left(\prod_{s \neq \tau} p(y_s|\theta_0, \xi_s) \right) a_\tau(h_T) \right] \quad (122)$$

$$= \sum_{\tau=1}^T \mathbb{E}_{p(\theta_{0:L})} \left[\mathbb{E}_{p(h_{\tau-1}|\theta_0, \pi_\phi)} \left[\sum_{h_T|h_{\tau-1}} \left(\prod_{s > \tau} p(y_s|\theta, \xi_s(h_{s-1})) \right) a_\tau(h_T) \right] \right] \quad (123)$$

where we have turned the sum over the variables up until τ into an expectation. In this form, we sample a single initial history $h_{\tau-1}$ and then sum over all histories that share that initial sequence, indicated by the sum over $h_T|h_{\tau-1}$. It is also possible to take an expectation over the future trajectories, but now we must note that we cannot take the expectation over y_τ itself as it is not present in the product. We obtain the following

$$\sum_{\tau=1}^T \mathbb{E}_{p(\theta_{0:L})} \left[\mathbb{E}_{p(h_{\tau-1}|\theta_0, \pi_\phi)} \left[\sum_{(\xi_\tau, y_\tau)|h_{\tau-1}} \mathbb{E}_{p(h_T|h_\tau, \theta_0, \pi)} [a_\tau(h_T)] \right] \right]. \quad (124)$$

Finally, we note that the sum over $(\xi_\tau, y_\tau)|h_{\tau-1}$ can be simplified to a sum over y_τ , since $\xi_\tau = \pi_\phi(h_{\tau-1})$ is computed deterministically. This gives the gradient expression stated in the Lemma.

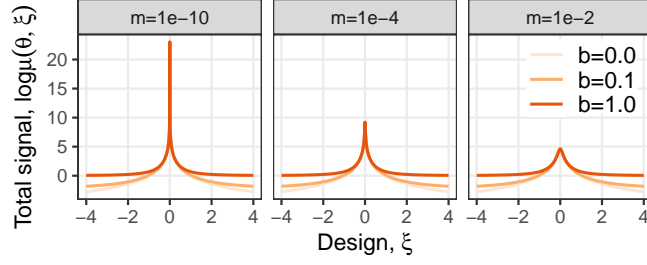


Figure 4. Log-total intensity

To form an unbiased estimator of (116), we use the estimator

$$\sum_{\tau=1}^T \sum_{y_{\tau}} a_{\tau}(h_T(\tau, y_{\tau})) \quad (125)$$

where we sample $h_T(\tau, y_{\tau})$ as follows. For a given τ , we sample a single history up until $h_{\tau-1}$, then fork into $|\mathcal{Y}|$ different paths depending on the value of y_{τ} , and continue to sample the history from $\tau + 1$ onwards. This is then done for each $\tau = 1, \dots, T$, to give a total cost of $\mathcal{O}(|\mathcal{Y}|T)$. This completes the proof. \square

D. Experiment details

Our experiments were implemented using PyTorch (Paszke et al., 2019) and Pyro (Bingham et al., 2018). We include code for each experiment in the Supplement. For full details on running the code, see instructions in the README.md file.

D.1. Location Finding

In this experiment we have K hidden objects or *sources* in \mathbb{R}^d , $d \in \{1, 2, 3\}$ and aim to learn their locations, $\theta = \{\theta_k\}_{k=1}^K$. The number of sources, K , is assumed to be known. Each of the sources emits a signal with intensity obeying the inverse-square law. In other words, if a source is located at θ_k and we perform a measurement at a point ξ , the signal strength will be proportional to $\frac{1}{\|\theta_k - \xi\|^2}$.

Since there are multiple sources, we consider the total intensity at location ξ , which is a superposition of the individual ones

$$\mu(\theta, \xi) = b + \sum_{k=1}^K \frac{\alpha_k}{m + \|\theta_k - \xi\|^2}, \quad (126)$$

where α_k can be known constants or random variables, $b, m > 0$ are constants controlling background and maximum signal, respectively. Figure 4 shows the effect b and m have on log-total signal strength.

We place a standard normal prior on each of the location parameters θ_k and we observe the log-total intensity with some Gaussian noise. We therefore have the following prior and likelihood:

$$\theta_k \stackrel{\text{i.i.d.}}{\sim} N(0_d, I_d), \quad \log y \mid \theta, \xi \sim N(\log \mu(\theta, \xi), \sigma) \quad (127)$$

The model hyperparameters used in our experiments can be found in the table below.

Parameter	Value
Number of sources, K	2
Base signal, b	10^{-1}
Max signal, m	10^{-4}
α_1, α_2	1
Signal noise, σ	0.5

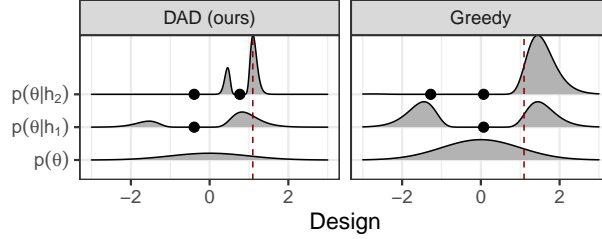


Figure 5. Posterior distributions of the location finding example with $K = 1$ source \mathbb{R} .

We trained a DAD network to amortize experimental design for this problem, using the neural architecture outlined in Section 4.3. Both the encoder and the decoder are simple feed-forward neural networks with a single hidden layer; details in the following table. For the encoder

Layer	Description	Dimension	Activation
Input	ξ, y	3	-
H1	Fully connected	256	ReLU
Output	Fully connected	16	-

and for the emitter

Layer	Description	Dimension	Activation
Input	$R(h_t)$	16	-
H1	Fully connected	4	-
Output	ξ	4	-

We optimized this network using Adam (Kingma & Ba, 2014) with exponential learning rate annealing with parameter γ . Full details are given in the following table.

Parameter	Value
Inner samples, L	2000
Outer samples	2000
Initial learning rate	10^{-4}
Betas	(0.9, 0.999)
γ	0.8
Gradient steps	10000
Annealing frequency	1000

To evaluate the stability between different training runs, we trained 10 DAD networks, computing the lower and upper bounds and a standard error based on these 10 runs:

$$\mathcal{L}_T(\pi) \pm 1s.e = 9.82 \pm 0.08 \quad (128)$$

$$\mathcal{U}_T(\pi) \pm 1s.e = 10.0 \pm 0.14 \quad (129)$$

Discussion details. We calculate the true optimal myopic (greedy) baseline using numerical integration. Since we are in $K = 1$ source in \mathbb{R} , the latent variable θ is one dimensional, allowing us to evaluate Equation (1) using line integrals as follows

$$I_t(\xi) = \int p(\theta|h_{t-1})\mathbb{E}_{p(y|\theta)} \left[\log \frac{p(y|\theta)}{\int p(\theta'|h_{t-1})p(y|\theta')d\theta'} \right] d\theta \quad (130)$$

$$= \int p(\theta|h_{t-1})\mathbb{E}_{p(y|\theta)} \left[\log \int p(\theta'|h_{t-1})p(y|\theta')d\theta' \right] d\theta + C \quad (131)$$

where $C = -H(p(y|\theta))$ is the entropy of a Gaussian, location independent and therefore constant with respect to ξ . We calculate (131) for a range of designs, $\xi \in \Xi_{\text{grid}}$, and select the optimal design $\xi^* = \arg \max_{\Xi_{\text{grid}}} I_t(\xi)$. The integrals

themselves are also calculated using numerical integration on a grid, Θ_{grid} , and use sampling to calculate the inner expectation; further details can in the table below.

Parameter	Value
Design grid, Ξ_{grid}	300 equally spaced from -3 to 3
θ grid, Θ_{grid}	600 equally spaced from -4 to 4
y samples for inner expectation	400

It is important to emphasize that even in this simple one-dimensional setting evaluating the myopic strategy is extremely costly and may require more sophisticated numerical integration techniques (e.g. quadrature) as posteriors become more peaked. Furthermore, as Figure 5 indicates, the resulting posteriors are complex and multi-modal even in 1D. This multi-modality may also be a reason why the variational method does not work well in this example.

D.2. Hyperbolic temporal discounting

We consider a hyperbolic temporal discounting model (Mazur, 1987; Vincent, 2016; Vincent & Rainforth, 2017) in which a participant’s behaviour is characterized by the latent variables $\theta = (k, \alpha)$ with prior distributions

$$\log k \sim N(-4.25, 1.5) \quad \alpha \sim \text{HalfNormal}(0, 2) \tag{132}$$

where the HalfNormal distribution is a Normal distribution truncated at 0. For given k, α , the value of the two propositions “£ R today” and “£100 in D days” with design $\xi = (R, D)$ are given by

$$V_0 = R, \quad V_1 = \frac{100}{1 + kD}. \tag{133}$$

The probability of the participant selecting the second option, V_1 , rather than V_0 is then modelled as

$$p(y = 1 | k, \alpha, R, D) = \epsilon + (1 - 2\epsilon)\Phi\left(\frac{V_1 - V_0}{\alpha}\right) \tag{134}$$

where Φ is the c.d.f. of the standard Normal distribution, i.e.

$$\Phi(z) = \int_{-\infty}^z \frac{1}{\sqrt{2\pi}} \exp\left(-\frac{1}{2}z^2\right) \tag{135}$$

and we fix $\epsilon = 0.01$. We considered the iterated version of this experiment, modelling $T = 20$ experiments with each sampled setting for the latents k, α .

We began by training a DAD network to amortize experimental design for this problem. The design parameters R, D have the constraints $D > 0$ and $0 < R < 100$. We represented R, D in an unconstrained space ξ_d, ξ_r and transformed them using the maps

$$D = \exp(\xi_d) \quad R = 100 \text{ sigmoid}(\xi_r) \tag{136}$$

We used the neural architecture outlined in Section 4.3. For the encoder E_{ϕ_1} we used the following network with two hidden layers

Layer	Description	Dimension	Activation
Design input	ξ_d, ξ_r	2	-
H1	Fully connected	128	Softplus
H2	Fully connected	128	Softplus
H3	Fully connected	4	-
H3'	Fully connected	4	-
Output	$y \odot H3 + (1 - y) \odot H3'$	4	-

The emitter network F_{ϕ_2} similarly used two hidden layers as follows

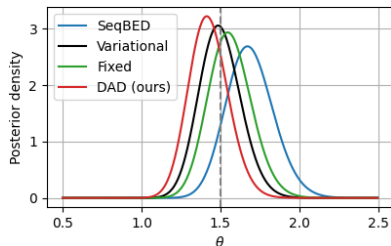


Figure 6. Comparison of posteriors obtained from a single rollout of the Death Process, used to compute the information gains quoted in Section 6.3. The dashed line indicates the true value $\theta = 1.5$ used to simulate responses.

Layer	Description	Dimension	Activation
Input	$R(h_t)$	4	-
H1	Fully connected	128	Softplus
H2	Fully connected	128	Softplus
Output	ξ_d, ξ_r	2	-

We optimized this network using SGD with momentum with exponential learning rate annealing with parameter γ . Full details are given in the following table

Parameter	Value
Inner samples, L	250
Outer samples	250
Initial learning rate	10^{-5}
Momentum	0.9
γ	0.96
Gradient steps	100000
Annealing frequency	1000

For the fixed baseline, we used the same optimization settings, except we set the initial learning rate to 10^{-1} . We trained the DAD and fixed methods on a machine with 8 Intel(R) Xeon(R) CPU E5-2637 v4 @ 3.50GHz CPUs, one GeForce GTX 1080 Ti GPU, 126 GiB memory running Fedora 32. Note this is *not* the machine used to conduct speed tests. For the Badapted baseline of Vincent & Rainforth (2017), we used the public code provided at <https://github.com/drbenvincent/badapted>. The slow method used 50 PMC steps with 100 particles and the fast method used 2 PMC steps with 20 particles. For the baselines of Frye et al. (2016) and Kirby (2009), we used the public code provided at <https://github.com/drbenvincent/darc-experiments-matlab/tree/master/darc-experiments>. These methods do not involve a pre-training step, except that we did not include time to compute the first design ξ_1 within the speed test, as this can be computed before the start of the experiment.

To implement the deployment speed tests fairly, we ran each method on a lightweight CPU-only machine, which more closely mimics the computer architecture that we might expect to deploy methods such as DAD on. The specifications of the machine we used are described below

Memory	7.7GiB
Processor	Intel® Core™ M-5Y10c CPU @ 0.80GHz × 4
Operating System	Ubuntu 16.04 LTS

The values in Table 2 show the mean and standard error of the times observed from 10 independent runs on a idle system. To make the final evaluation for each method in Table 3, we computed the sPCE and sNMC bounds using $L = 5000$ inner samples and 10000 outer samples of the outer expectation. We present the mean and standard error from the outer expectation over 10000 rollouts.

D.3. Death process

For the Death Process model (Cook et al., 2008), we use the settings that were described by Kleinegesse et al. (2020). Specifically, we use a truncated Normal prior for the infection rate

$$\theta \sim \text{TruncatedNormal}(\mu = 1, \sigma = 1, \min = 0, \max = \infty). \tag{137}$$

The likelihood is then given by

$$\eta = 1 - \exp(-\xi\theta) \quad y|\theta, \xi \sim \text{Binomial}(N, \eta) \tag{138}$$

where we set $N = 50$. We consider a sequential version of this experiment as in Kleinegesse et al. (2020), with $T = 4$ and in which an independent stochastic process is observed at each step, meaning there are no constraints relating ξ_1, \dots, ξ_4 other than the natural constraint $\xi_t > 0$.

We began by training a DAD network to perform experimental design for this problem. We used the neural architecture outlined in Section 4.3. For the encoder E_{ϕ_1} we used the following network with two hidden layers

Layer	Description	Dimension	Activation
Input	ξ, y	2	-
H1	Fully connected	128	Softplus
H2	Fully connected	128	Softplus
Output	Fully connected	16	-

The emitter network F_{ϕ_2} similarly used two hidden layers as follows

Layer	Description	Dimension	Activation
Input	$R(h_t)$	16	-
H1	Fully connected	128	Softplus
H2	Fully connected	128	Softplus
Output	ξ	1	Softplus

We optimized this network using SGD with momentum with exponential learning rate annealing with parameter γ . Full details are given in the following table

Parameter	Value
Inner samples, L	100
Outer samples	100
Initial learning rate	0.03
Momentum	0.9
γ	0.9
Gradient steps	100000
Annealing frequency	1000

For the fixed baseline, we used the same optimization settings, except we set the initial learning rate to 10^{-1} and we set $\gamma = 0.85$. We trained the DAD and fixed methods using the same machine as used for training in Section D.2. For the variational baseline, we used a truncated Normal variational family to approximate the posterior at each step. We used SGD with momentum to optimize the design at each step, and to optimize the variational approximation to the posterior at each step. We used exponential learning rate annealing with parameter γ . The settings used were

Parameter	Value
Design inner samples	250
Design outer samples	250
Design initial learning rate	10^{-2}
Design γ	0.9
Design gradient steps	5000
Inference initial learning rate	10^{-3}
Inference γ	0.2
Inference gradient steps	5000
Momentum	0.1
Annealing frequency	1000

For the SeqBED baseline, we used the code publicly available at <https://github.com/stevenkleinmesse/seqbed>. The speed tests except for SeqBED were implemented as in Section D.2. For SeqBED and the variational method, we did not include the time to compute the first design as deployment time, as this can be computed before the start of the experiment. Due to its long-running nature, we implemented the speed test for SeqBED using a more powerful machine with 40 Intel(R) Xeon(R) CPU E5-2680 v2 @ 2.80GHz processors and 189GiB memory. Therefore, the timing value for SeqBED given in Table 4 represents a significant *under-estimate* of the expected computational time required to deploy this method. However, we note that SeqBED can be applied to a broader class of implicit likelihood models.

For evaluation of $\mathcal{I}_4(\pi)$ in the Death Process, it is possible to compute the information gain $H[p(\theta)] - H[p(\theta|h_T)]$ to high accuracy using numerical integration. We then took the expectation of the information gain over rollouts, see Table 4 for the exact number of rollouts used. This gives us an estimate

$$\mathcal{I}_4(\pi) = \mathbb{E}_{p(h_T|\pi)} [H[p(\theta)] - H[p(\theta|h_T)]] \tag{139}$$

which is shown to be a valid form for the total EIG in Section A.

For a comparison with SeqBED which is too slow to use this evaluation, we instead performed one rollout of each of our methods using a fixed value $\theta = 1.5$. This is close in spirit to the evaluation used in Kleinmesse et al. (2020). Figure 6 shows the posterior distributions obtained from this rollout. The information gains were then computed using the aforementioned numerical integration and are quoted in Section 6.3. We observe that visually the posterior distributions are similar, and cluster near to the true value of θ .